Me 159

ACTA POLYTECHNICA SCANDINAVICA

MECHANICAL ENGINEERING SERIES No. 159

Tribology of Prosthetic Joints – Validation of Wear Simulation Methods

OLOF CALONIUS

Helsinki University of Technology
Department of Mechanical Engineering
Laboratory of Machine Design
P.O. Box 4300
FIN-02015 HUT
FINLAND

Dissertation for the degree of Doctor of Science in Technology to be presented with due permission of the Department of Mechanical Engineering, for public examination and debate in Auditorium K216 at Helsinki University of Technology (Espoo, Finland) on the 4th of October, 2002, at 12 o'clock noon.

ESPOO 2002

Calonius, O., **Tribology of prosthetic joints – validation of wear simulation methods.** Acta Polytechnica Scandinavica, Mechanical Engineering Series No. 159, Espoo 2002, 62 pp. Published by the Finnish Academies of Technology. ISBN 951-666-603-5. ISSN 0001-687X.

Keywords: prosthetic joint, polyethylene, wear particles, slide track

ABSTRACT

In hip and knee arthroplasty, loosening of prosthetic components is the principal reason for expensive and complicated reoperations. Loosening is believed to be caused mainly by tissue reactions to wear particles removed from ultrahigh molecular weight polyethylene bearing surfaces. The tissue reactions, leading to bone loss, depend on the size and amount of the particles. Wear simulators are important in the evaluation of prosthetic joints and their materials. The validation of a simulation is based on the comparison of wear rates and wear mechanisms with clinical findings. Polyethylene wear particles from two different hip simulators, a pin-on-disk hip wear device, and a knee wear simulator, were examined using digital image analysis. The average equivalent circle diameter of the particles was 0.10–0.69 μm, which corresponded well with published clinical studies. The particle size distribution was influenced by crosslinking, counterface roughness, and type of simulation (hip or knee). The kinematics of the hip joint in walking, and of ten contemporary hip simulators was analyzed. To this end, software for computing tracks drawn on the counterface by arbitrary points of the bearing surface, the so-called slide tracks, was developed and experimentally verified. The slide track pattern, produced by many points, illustrated the relative motion. Walking was shown to result in open slide tracks on the center of contact, implying continually changing direction of sliding. This phenomenon, known to be crucial for valid wear simulation, was reproduced by simulators having abduction-adduction motion in addition to flexion-extension motion. The most widely used hip simulator, commonly referred to as biaxial, was found to be actually three-axial. The new method can be further utilized, e.g., for computing an improved wear factor involving the variation of relative motion and contact pressure with location.

© All rights reserved. No part of this publication may be reproduced, stored in a retrieval system, or transmitted, in any form or by any means, electronic, mechanical, photocopying, recording, or otherwise, without the prior permission of the author.

PREFACE

This thesis presents some of the research work done during the years 2000–2002 in the field of biotribology at the Laboratory of Machine Design of Helsinki University of Technology. The research was headed by Dr. Vesa Saikko and funded by the Academy of Finland. The Department of Mechanical Engineering provided funding for finalizing the thesis. My postgraduate studies were funded by Skanaluminium, Finnyards Ltd. and Kværner ASA. The financial support is gratefully acknowledged.

I would like to thank Professor Mauri Airila for the opportunity to start working as a researcher at the laboratory, and for continuous support and encouragement throughout the course of building this thesis. The thesis work was supervised by Dr. Saikko, to whom I would like to express my sincere gratitude for accepting me in his research team, and for the advice and unlimited expertise offered for my guidance. Further, I would like to thank the pre-examiners, Professor Kenneth Holmberg and Dr. Claude Rieker for the time and interest taken in reviewing my thesis, and for their knowledgeable comments. I would like to thank Dr. Tiina Ahlroos for cooperation and support during the postgraduate studies and the research work, Mr. Jaakko Keränen for scanning electron microscopy and Mrs. Elizabeth Heap-Talvela for checking the English language.

Part of my postgraduate studies were done at the Norwegian University of Science and Technology (NTNU) during the years 1998–2000. I am greatly indebted to Professor Torgeir Moan for providing me with the opportunity to study at the Department of Marine Structures and improve my skills in mechanics of materials, and particularly welding mechanics, under the auspices of the Aluminium in Ship project. The activities included measurements of welding deformations with digital photogrammetry, and numerical welding simulations with time-dependent, non-linear thermo-mechanical finite element analyses. I would like to thank Professor Matti Kleimola and Mr. Toralf Cock, who arranged for me to take part in the Skanaluminium scholarship program, through which I had the opportunity to study engineering design and aluminium materials science, in courses held at NTNU in Trondheim, and Kungliga Tekniska Högskolan (KTH) in Stockholm. The studies of aluminium structures gave me the possibility to work in close cooperation with industry, by actively taking part in planning and negotiating large-scale research projects (with Finnyards Ltd.), and doing actual research work (with Kværner Fjellstrand AS). The experience acquired during that time has been of great value in my present research work.

Otaniemi, May 2002

Olof Calonius

CONTENTS

LIST OF PUBLICATIONS

This dissertation consist of a summary and the following publications:

I Saikko, V., Ahlroos, T. and Calonius, O., A three-axis knee wear simulator with ball-on-flat contact. Wear Vol. 249 (2001), p. 310–315.

II Saikko, V., Ahlroos, T., Calonius, O. and Keränen, J., Wear simulation of total hip prostheses with polyethylene against CoCr, alumina and diamond-like carbon. Biomaterials Vol. 22 (2001), p. 1507–1514.

III Saikko, V., Calonius, O. and Keränen, J., Effect of counterface roughness on the wear of conventional and crosslinked ultrahigh molecular weight polyethylene studied with a multidirectional motion pin-on-disk device. J Biomed Mater Res, Vol. 57 (2001), p. 506–512.

IV Calonius, O. and Saikko, V., Analysis of polyethylene particles produced in different wear conditions in vitro. Clin Orthop, Vol. 399 (2002), p. 219–230.

V Saikko, V. and Calonius, O., Slide track analysis of the relative motion between femoral head and acetabular cup in walking and in hip simulators. J Biomech Vol. 35 (2002), p. 455–464.

VI Calonius, O. and Saikko, V., Slide track analysis of eight contemporary hip simulator designs. J Biomech Vol. 35 (2002), p. 1439–1450.

THE AUTHOR'S CONTRIBUTION

All publications included in the dissertation are the result of a group effort. In Publications I–IV, the doctoral candidate was responsible for the wear particle analyses. The candidate independently performed all digital image analyses and produced all wear particle statistics. In Publications V and VI, the candidate was responsible for developing and programming all the functions that constituted the slide track software, and for performing the slide track analyses.

Reference [12] is based directly on the method of computation presented in Publication V and is closely related to the research reported in the dissertation. In this paper, which has been submitted for publication in the Journal of Biomechanics, the candidate is the first author and he contributed with additional programming and performed the force track computations.

ORIGINAL FEATURES

This thesis treats the validation of wear simulation of prosthetic joint materials, particularly ultrahigh molecular weight polyethylene. The following features and findings are believed to be original:

1. A verified method of computing slide tracks, visualizing and quantifying the relative motion at the articulation of the hip joint, was developed. The method made it possible to compute the motion of marker points on the acetabular cup or the femoral head on the counterface. New features of the method were:
   - Marker point rotations were made according to the Euler rotation sequence determined by analyzing the simulator or the biomechanical electrogoniometer.
   - The number of marker points and their locations on the surface of articulation were not restricted.
   - Track points were computed by repeatedly rotating the marker points from their neutral position to their instantaneous track position according to the values of the Euler rotation angles of each time step, which prevented the accumulation of numerical errors.
   - Plane figures of the slide track patterns were made by a flattening procedure which minimized the distortion of each track figure.

2. Computed slide tracks were experimentally verified by engraving and drawing the tracks on the femoral head in two different hip simulators.

3. The correct (experimentally verified) slide track pattern of the so-called biaxial rocking motion (BRM) simulator (also known as the orbital bearing machine, OBM) was presented. The verified pattern differed from the pattern presented earlier by another research group.

4. For the BRM (OBM) simulator, it was shown that the shape of the rotation-prevention lever affected the slide track pattern. This has led to the realization that the shape of the lever determined whether internal-external rotation (IER) motion was present, and that the most popular type of this simulator is not biaxial, but in fact three-axial.

5. Slide tracks were computed for motion waveforms presented in the ISO/DIS 14242-1 standard.

6. Polyethylene wear particle analyses were conducted for the first time for wear simulators functioning according to the following principles:
   - Circularly translating pin-on-disk (CTPOD) hip wear device with static load.
   - Genuinely biaxial rocking motion hip wear simulator with zero-offset rotation prevention lever (HUT-BRM) and static load.
   - Ball-in-socket hip joint simulator (HUT-3) with dynamic load and three-axis motion similar to what has been recorded for gait.
   - Ball-on-flat knee wear simulator with three-axis motion and static load.

   It was verified that the particles were similar in size and shape to those isolated from tissue samples obtained at revision operations. In all simulators, the majority of the particles were smaller than 1 μm. In the knee wear simulator, the particles were larger on average than particles from hip wear simulators, which was in agreement with clinical findings.

7. Factors with a significant influence on the average polyethylene wear particle size were the counterface surface roughness and the type of polyethylene (conventional or crosslinked). The effect of the polished counterface material on the average wear particle size was weak. The following table summarizes the effects:

Counterface material	Polyethylene type	Surface roughness R_a (μm)	Particle size *ECD* (μm)
CoCr	Conventional	0.022	0.21
CoCr	Crosslinked	0.014	0.10
CoCr	Conventional	0.24	0.37
CoCr	Crosslinked	0.22	0.39
Al_2O_3	Conventional	0.01	0.27
CoCr	Conventional	0.01	0.33
DLC	Conventional	0.01	0.33

NOMENCLATURE

AA	Abduction-adduction
APT	Anterior-posterior translation
BOF	Ball-on-flat (knee wear simulator)
BRM	Biaxial rocking motion (hip wear simulator)
CTPOD	Circularly translating pin-on-disk (wear test device)
DLC	Diamond-like carbon
FE	Flexion-extension
FTIR	Fourier transform infrared (spectroscopy)
HUT-3	Helsinki University of Technology hip joint simulator Mark III
HUT-BRM	Helsinki University of Technology BRM simulator
IER	Internal-external rotation
IOR	Inward-outward rotation (same as IER)
OBM	Orbital bearing machine (same as BRM simulator)
PMMA	Polymethylmethacrylate (bone cement)
PTFE	Polytetrafuoroethylene
SEM	Scanning electron microscopy
UHMWPE	Ultrahigh molecular weight polyethylene

Aspect ratio	Major dimension divided by minor dimension of wear particle or slide track
Force track	Track made on the counterface by the point of joint contact resultant force
In vitro	Process or phenomenon studied under laboratory conditions
In vivo	Within the living organism
Slide track	Track made on the counterface by a point on the surface of femoral head or acetabular cup due to cyclic relative motion

A	Projected area of wear particle
AR	Aspect ratio
d_{max}	Major diameter of wear particle
d_{min}	Minor diameter of wear particle
ECD	Equivalent circle diameter
FF	Form factor

k	Wear factor; $k = (V/n) / \int L\mathrm{d}x$
L	Joint contact resultant force
n	Number of cycles
p	perimeter of wear particle
r	Radius of femoral head
R	Roundness
t	Time
T	Cycle time
V	Wear volume
x	Sliding distance; track coordinate
α	FE angle in computations; $\alpha > 0$ corresponds to extension
β	AA angle in computations; $\beta > 0$ corresponds to abduction
γ	IER angle in computations; $\gamma > 0$ corresponds to internal rotation
τ_μ	Tangential shear stress at articulating surface caused by friction
ψ	Angle of inclination of femoral head in BRM simulator

1 INTRODUCTION

1.1 General

Biotribology offers a challenging, multidisciplinary field of research, involving orthopedics, biomechanics, materials science and tribology. The science of tribology studies the friction, wear and lubrication of interacting surfaces in relative motion. Friction is the resistance to relative sliding or rolling motion of the surfaces. Overcoming friction dissipates energy and causes wear of the surfaces. Lubrication provides an effective means of reducing friction and wear by separating contacting solids with a thin layer of material of low shear strength. The purpose of tribological research of prosthetic joints is to minimize friction and wear of the implant, and thereby to increase the lifetime of the joint.

Human joints are normally tribologically excellent, they have a very low friction coefficient and the cartilaginous surfaces can last in excess of 70 years [22]. The joint may, however, become damaged through injury, disease or unusual loading and motion. In 1999, the most common reasons for primary hip and knee arthroplasties were arthrosis and rheumatoid arthritis, according to the National Agency for Medicines in Finland [40]. Total joint replacement arthroplasty can provide the patient with dramatically improved quality of life by relieving pain and offering increased mobility. A failed prosthesis however, causes pain and reduces the ability to work and necessitates a revision operation. These complex and expensive revision operations are a great concern for the public health care. The most common reason for revision operation was loosening of the components (66% of hip revisions and 20% of knee revisions). Other reasons for revision included infection, luxation, bone fracture and malpositioning. The number of operations performed is shown in Table I, together with the survival percentage of cemented prostheses 7-10 years after operation [40]. The outcome of a revision operation is often worse than that of a primary operation, with lower survival rate and thus a need for a second revision in a few years´ time. The number of revision operations could be reduced if loosening of the prostheses could be prevented. The current understanding is that loosening is primarily due to bone loss around the implant, caused by adverse tissue reactions to wear particles [29]. An alternative explanation for loosening is that osteolysis is caused by fluid pressure in the fibrous membrane that will develop around the cement securing the prosthesis [2]. However, even if high pressures during motion can play a part in killing bone cells, particles are still involved in inhibiting bone formation [26]. In fact, a recent study [36] concludes that both particles and pressure are important factors that can contribute to osteolysis, and that especially their combined effect could accelerate implant loosening. Therefore, it appears that wear has a

major role in limiting the lifetime of prostheses, justifying the research effort in development of wear resistant materials and wear simulation equipment for pre-clinical evaluation of these materials.

Table I. Total hip and knee arthroplasties in Finland in 1999 [40]

Joint	Operations			Survival percentage [a]	
	Primary	Revision	Total	Primary [b]	Revision
Hip	4742	1158	5900	87	75
Knee	4380	409	4789	93 [c]	81 [d]

[a] Survival percentage of most used cemented prostheses types ten years after operation

[b] Reason for operation was arthrosis; [c] Nine years after primary operation; [d] Seven years after revision operation

Hip joint replacement has been dominated by implants with metal femoral heads and acetabular cups made of a polymeric material since Sir John Charnley introduced the low-friction arthroplasty (LFA) in the late 1950s. The idea was to use a material pair with very low interfacial friction and a femoral head with much smaller diameter than in the natural hip joint. These measures would substantially reduce the frictional torque and thereby increase the lifetime of the implant, by reducing the tendency to loosening at the implant-bone interface. In addition, Charnley used generous amounts of acrylic bone cement to secure the fixation of the implant [23]. However, the problem of polymer wear quickly emerged. The first Charnley prostheses had an acetabular cup made of polytetrafluoroethylene (PTFE). The wear of the PTFE cup was so severe that the stainless steel femoral head penetrated through the radial thickness of the cup in only three years. The PTFE cup was changed to a cup made of ultrahigh molecular weight polyethylene (UHMWPE), and the wear rate dropped dramatically [17,19,20]. In a study with patients younger than forty years at the time of operation, the average wear of the acetabular component of the Charnley prostheses was 0.19 mm/year for components that were eventually revised, while it was 0.09 mm/year for components that were functioning well [58]. The wear was measured from radiographs as penetration of the femoral head into the acetabular cup. The wear rates imply that it would take many decades for the head to wear through the cup. However, failure of the prosthesis due to wear through of the polyethylene component is seldom the reason for revision. The main factor limiting the lifetime of the prosthesis has been osteolysis and loosening of the implant. Initially, it was

thought that the osteolysis was due to the use of acrylic bone cement in fixation of the implant. Later, it was discovered that loosening was not due to the 'cement disease', but rather due to polyethylene wear particles [19].

Briefly, the implant loosening is thought to proceed as follows [8,29]. The tissues around the implant react to polyethylene wear particles by activating the immune defense system. Macrophages in the tissues will try to engulf and destroy (phagocytose) the particles. However, the polyethylene particles are not degradable like bacteria or other micro-organisms. The body nevertheless reacts by summoning more and more cells to the site to eliminate the particles, resulting in granuloma. Multi-nucleated giant cells are formed when macrophages fuse together while isolating the particles from surrounding tissue. Macrophages either influence resorption of bone directly, or by adversely influencing the normal bone remodeling process. Normally, osteoclasts dissolve bone mineral and subsequently osteocytes and osteoblasts lay down new bone where the osteoclasts have been active. Due to the wear debris, macrophages release chemical messages, cytokines, which activate the osteoclasts and bone loss may result. Particles with a size ranging from 0.2 μm to 8 μm have been found to be the most active, biologically [27,29]. In addition to the size of the particles, the number of the particles will influence the incidence of osteolysis. According to a study by Revell et al. [45], the critical number of particles for osteolysis is 1×10^{10} particles per gram tissue.

1.2 Properties of polyethylene in prosthetic joints

UHMWPE is a semicrystalline polymer with crystalline domains contained in an amorphous matrix. The crystalline phase consists of folded rows of carbon atoms, grouped together in the form of lamellae that are of the order of 0.01 μm to 0.05 μm in thickness and 10 μm to 50 μm in length. The amorphous phase consists of tangled and randomly oriented polymer chains. Resistance to mechanical deformation is provided by tie molecules that interconnect the lamellae. The average molecular weight of UHMWPE is $3.5–6 \times 10^6$ g/mol. UHMWPE stock material is typically manufactured by either ram extrusion or compression molding. Actual components are made by turning and milling operations. Alternatively, UHMWPE resin can be converted into near net shape by direct compression molding using individual molds. Young's modulus is typically of the order of 1 GPa and yield strength of the order of 20 MPa. [32,34]

Sterilization by irradiation significantly affects the long-term wear properties of UHMWPE. Earlier, the sterilization was done in air with a gamma radiation dose of 25 to 40 kGy. However, irradiation in air, and subsequent shelf aging, degraded the properties of the UHMWPE. As a result

of irradiation, free radicals are formed in the material. Some of the free radicals recombine and form crosslinks, while others remain reactive and cause oxidation damage of the material over long periods of time. Because oxidation damage of the UHMWPE component can lead to catastrophic wear, gamma irradiation in air has now been abandoned as a method of sterilization [34]. Instead, sterilization is done in nitrogen or argon, or without ionizing radiation using ethylene oxide (EtO) gas, or gas plasma [7]. These methods do not reduce the wear resistance of UHMWPE, but there are other problems involved. EtO is toxic and a long time is required to sterilize the components, while gas plasma is a newly introduced method and not much clinical validation is available yet. Crosslinking, as such, does improve the wear resistance of the UHMWPE. Therefore, manufacturers have developed methods of crosslinking that do not lead to oxidation damage. Although UHMWPE can be chemically crosslinked, in orthopedic applications the focus has been on crosslinking by ionizing radiation, followed by a thermal treatment to stabilize the free radicals. Both gamma and electron beam irradiation have been used. Often the absorbed dose is much higher than the regular sterilization dose of 25–40 kGy. In some wear tests, the wear rate decreased with the radiation dose to an almost undetectable level at approximately 150 kGy [34]. The thermal treatment can involve heating the UHMWPE to above the melt temperature and keeping the material at around 150 °C for several hours. An alternative is to heat treat the material at temperatures of 37–50 °C for up to 144 hours [34]. Crosslinking improves the wear resistance of UHMWPE, especially against the multidirectional motion typical of the hip joint. However, in the knee joint, the relative motion is closer to linear reciprocating motion, and consequently crosslinking does not necessarily improve the wear resistance, which was reported in a knee simulator study by Wang et al. [64]. In this thesis, the wear of crosslinked UHMWPE was compared to the wear of conventional UHMWPE in Publication III.

1.3 Wear simulation of prosthetic materials

The objective of wear simulation is to improve the durability of prosthetic joints, by evaluating the wear performance of prospective implant materials under conditions that are – in a tribological sense – close to the conditions in vivo. This means that the essential features of the relative motion at the articulation, the lubrication and the loading, are taken into consideration when setting up the wear simulation equipment. There are different kinds of equipment depending on whether only materials, or actual prosthetic components, are being tested. Simple equipment, such as the pin-on-disk device, is affordable, and can be used for wear testing of materials provided that the motion is relevant, i.e., corresponds to the actual wear situation [11,48]. A large-capacity device, such as the

twelve-station CTPOD, can be used for studying the effect of varying factors, such as counterface surface roughness (Publication III) and lubricant protein content [51], on the wear in a single test. In slightly more complicated equipment, such as the BRM (OBM), actual prosthetic components can be tested. The relative motion and the loading are often simplified, to keep the cost of the equipment down. Full-featured joint simulators, such as the HUT-3, are more complicated in that they closely reproduce physiologic motion and use dynamic loading.

The wear simulation is run for several million cycles. In general, it is considered that one million cycles correspond to one year in vivo [22,62]. The running-in period encompasses approximately the first half a million cycles. The steady-state wear is assessed by measuring the wear after the running-in period. Wear is measured either gravimetrically by determining the weight loss of the component, or by measuring the volume of the material that has been removed, i.e., the wear pit dimensions. Lubricant absorption or creep of the loaded components, especially for polyethylene, is taken into account. Wear measurements are normally done at lubricant change stops, e.g., every 500 000 cycles.

1.4 Validation of wear simulation

The principal methods of evaluating prosthetic wear simulations, are measuring the amount of worn material, visual and microscopic inspection of the wear surfaces and microscopic analysis of the wear debris. These evaluations are done in connection with every wear test. Ultimately, wear simulation results are validated against results of in vivo radiological wear measurements, or by comparing to results of inspection and wear measurements of components retrieved at revision operations or autopsy. Simulator wear debris is compared to debris isolated from periprosthetic tissues. Since the effect of polyethylene wear particles on implant loosening is known [8,29,45], and since the relative motion of the articulating surfaces is known to influence the production of wear debris [48,60,64], analysis of relative motion must be considered an important part of validation. Motion analysis is preferably done in the simulator design stage, but can be applied in the evaluation of an existing simulator design, e.g., if the in vivo wear process is not sufficiently accurately reproduced [5,10]. In this thesis, the focus was on validation in terms of polyethylene wear debris (Publications I–IV) and analysis of relative motion of the hip joint (Publications V and VI).

Ultra high molecular weight polyethylene wear particles are very small, and therefore scanning electron microscopy is widely used for the characterization of the particles. First, the particles are isolated from samples of tissue or serum lubricant, using sodium or potassium

hydroxide digestion and filtration. Then, scanning electron micrographs are taken and subsequently processed, using image analysis software to obtain a particle size distribution. Differences in size distributions between particles from wear simulators and from tissues suggest that there could be fundamental differences in the wear conditions. [13,33,37,55]

Many studies have shown that only multidirectional motion yields realistic wear for polyethylene [10,48,60,62]. Multidirectional motion means that the direction of sliding changes many times during the motion cycle, unlike, e.g., the situation in a regular pin-on-disk wear test device, in which the relative motion is unidirectional. The cyclic relative motion of the hip joint can be illustrated by computing tracks made on the counterface by marker points on the surface of the femoral head or acetabular cup, the so-called slide tracks. The tangent to a slide track indicates the instantaneous direction of sliding. If the slide tracks are open loops (e.g., have an overall shape which is roughly elliptical) or figures of eight, the direction of sliding is changing continually, implying multidirectional motion. Linear slide tracks, or slide tracks with very high aspect ratio, suggest reciprocating (bi-directional) motion, in which polyethylene wear is nearly zero [48,62].

1.5 Objectives and scope of the thesis

The objective of the thesis was to validate the performance of the wear simulators in use at Helsinki University of Technology, in terms of size and shape of wear particles and type of relative motion of the articulation. To this end, the aim was to develop a procedure for determining the size distribution of wear particles isolated from lubricant used in the wear simulations. In addition, the objective was to develop a computer program that would make it possible to visualize and analyze the relative motion of the articulating surfaces of the hip joint. Earlier, the wear performance of the simulators had routinely been verified by gravimetric wear measurements and by microscopic analysis of wear of the surfaces. The present work was intended as a further validation of the obtained wear results and a basis for studies on the relationship between the type of relative motion and wear.

The motivation for the study was to verify that the same wear mechanisms were acting in the simulators as in vivo, by comparing particles isolated from the simulator lubricants with particles isolated from periprosthetic tissues. This was important, since it was known from previous research [48,49,60,61] that the type of motion and lubricant significantly influences the morphology and amount of wear debris. By studying the motion of the hip joint, it was possible to determine to what degree the slide track patterns of the simulators were different from each other, and from the pattern associated with walking. For this purpose, a systematic computational approach was needed. The

motion computations are a prerequisite for further numerical studies of wear related phenomena, including length and shape of force track, sliding speed, quantifying the changing direction of motion, and the integral $\int L\mathrm{d}x$, which is needed for determining the wear factor k.

The scope of the particle analysis was the wear of ultrahigh molecular weight polyethylene against a hard counterface. The simulators used in the wear tests were all designed by Dr. Saikko at the Laboratory of Machine Design at Helsinki University of Technology. They included an innovative pin-on-disk wear simulator design (CTPOD), a hip wear simulator (BRM or OBM), a knee wear simulator (BOF), as well as a hip joint simulator (HUT-3). The analysis focused on the morphology and the size distribution of the polyethylene particles. The scope of the slide track analysis was the relative motion of the articulating surfaces of the hip joint. The effort was directed at developing a computational tool to be used not only for visualizing the relative motion, but also for quantitative assessment of the relationship between motion of the articulating surfaces and polyethylene wear.

The thesis is organized as follows. After the Introduction, Chapter 2 is a summary of materials and methods of wear testing, particle analyses (Publications I–IV) and slide track analyses (Publications V and VI). Chapter 3 summarizes the results of the analyses. In Chapter 4, the results of the particle analyses are compared to clinical results, and the effects of wear conditions on size and shape of polyethylene particles are discussed. The results of the slide track analyses are compared to the results of another research group. The relation between relative motion and polyethylene wear is discussed. Chapter 5 presents the conclusions, as well as implications for future research. Appendix A is a brief summary of the slide track computations.

2 METHODS

In the following sections, a summary of the methods used in the analysis of polyethylene wear particles and slide tracks is given. When referring to the motion of the hip joint, the directions are named according to Figure 1, which is a frontal view of the right hip joint. The directions of motion of the ball-on-flat simulator are shown in Publication I, Fig. 2. Figure 2 is an overview of the wear particle analysis and Figure 3 of the slide track analysis. Wear particles isolated from used simulator lubricants were analyzed to verify that they were similar in size and shape to those found in clinical studies of particles isolated from periprosthetic tissues. The slide track computations were done to verify that the relative motion at the articulation involved continually changing direction of sliding,

which is known to be a crucial factor in obtaining the correct wear mechanisms for polyethylene in artificial hip and knee joints.

2.1 Wear particle analysis

Ultra high molecular weight polyethylene wear particles were isolated from used lubricant taken during tests with four different types of wear simulators. Three of the simulators were intended for research on wear of materials and components of hip prostheses. These included a circularly translating pin-on-disk (CTPOD) hip wear device [48], a biaxial rocking motion (BRM) hip wear simulator [49], and a full-featured three-axial hip simulator, the HUT-3 [47]. The fourth simulator type was a ball-on-flat (BOF) knee wear device (Publication I). Table II contains a summary of the wear simulators from which lubricant samples for particle analyses were taken. In addition, particles were isolated from synovial fluid aspirated at revision surgery of a prosthetic hip (Publication IV).

Table II. Wear simulators

Simulator	Contact geometry	Cycle	Range of motion				Force track		Loading	Ref./ Publ.
		f (Hz)	FE (deg)	AA (deg)	IER (deg)	APT (mm)	Shape	Length (mm)	Type and Value	
CTPOD	Flat-on-flat [(a)]	1.02	–	–	–	–	Circle	31.4	Static 70.7 N	[48]
BRM	Ball-in-socket	1	46	46	–	–	Circle	34.4 [(b)]	Static 1 kN	[49]
HUT-3	Ball-in-socket	1.18	46	12	12	–	Ellipse	24.2 [(b)]	Dynamic 0.35–3.5 kN [(c)]	[47]
BOF	Ball-on-flat	1.08	42.4	–	10	10	Figure of eight	20.1	Static 2 kN	(I)

[(a)] Relative motion is biaxial, not unidirectional; [(b)] For 28 mm head diameter
[(c)] Range used in test from which particles were isolated [49]

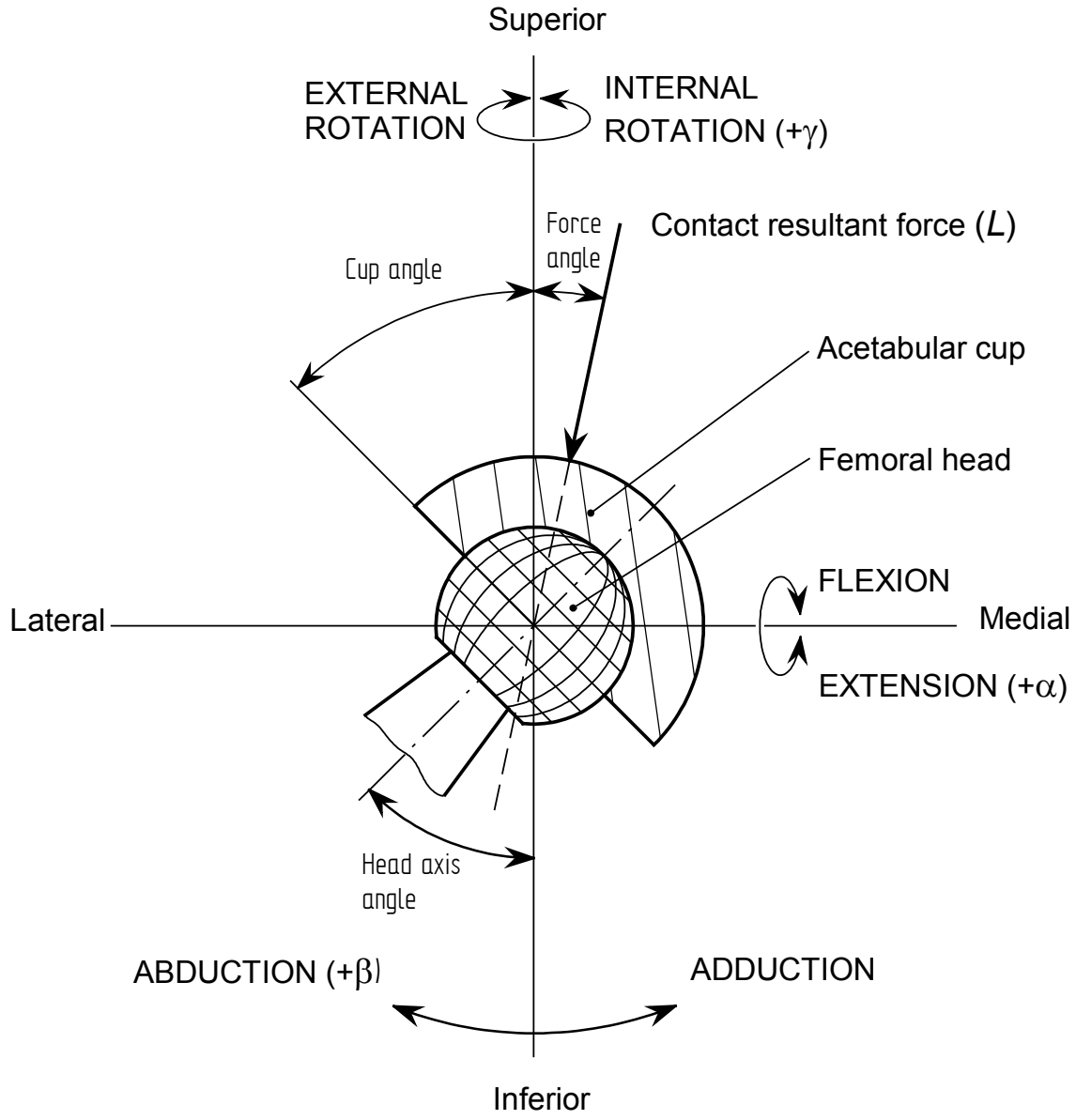

Antero-posterior view of right hip joint

Figure 1. Illustration of hip joint with directions of motions shown.

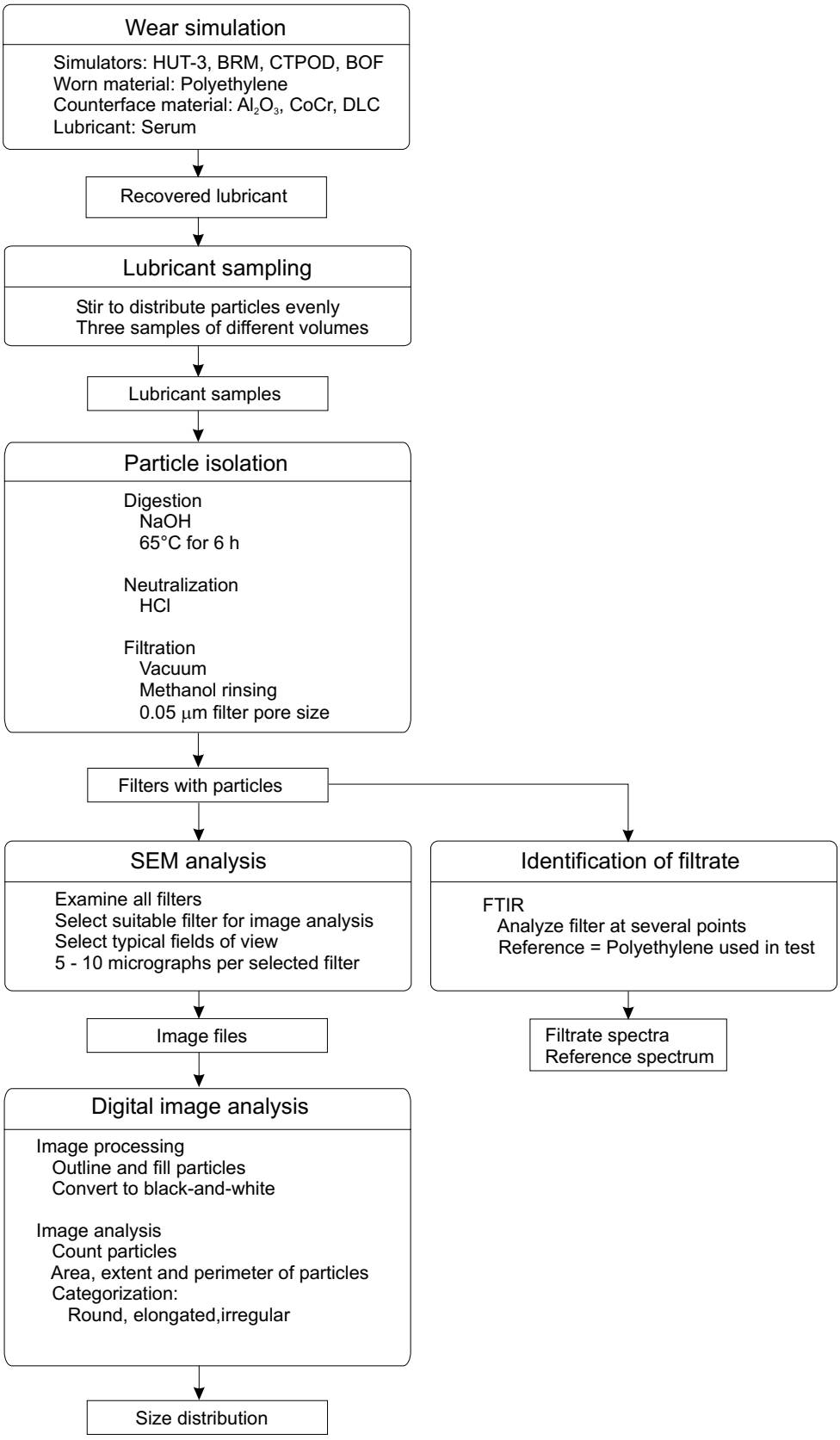

Figure 2. Overview of wear particle analysis.

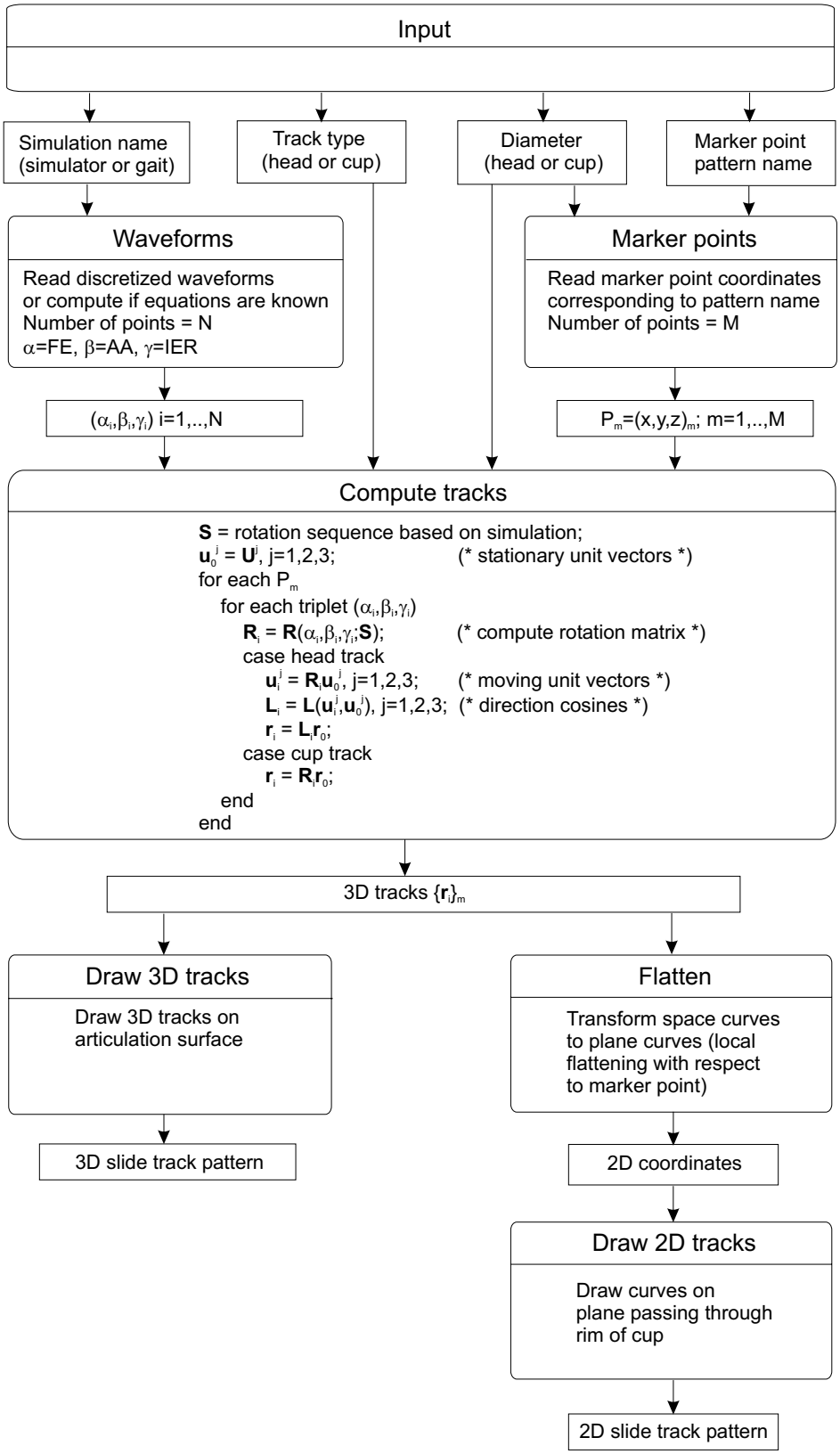

Figure 3. Overview of slide track computations. The effect of design changes in a simulator can be assessed by generating motion waveforms with different amplitudes or phases, or by changing the rotation sequence. A summary of the computations is given in Appendix A.

Table III. Lubricants

Lubricant	Starting solution	Dilution	Protein content (mg/ml)	Additive	Used in test with simulator	Ref. / Publ.
Bovine serum	Sigma B-2771	Undiluted	73	NaN_3	CTPOD	[50]
Bovine serum	Sigma B-2771	Distilled water 1:2	24	NaN_3	HUT-3	[49]
Calf serum	HyClone Alpha	Distilled water 1:1	21	–	BOF,BRM	(I,II)
Albumin	Sigma A-7534	0.15 M NaCl	40	NaN_3	CTPOD	[50]
Globulin	Sigma G-4904	0.15 M NaCl	10	NaN_3	CTPOD	[50]

In all simulators, serum lubrication was used. In addition, some CTPOD tests were run with albumin and gamma globulin solutions as lubricants, see Table III. In the tests, three types of polyethylene (non-irradiated, γ-irradiated and crosslinked) were worn against various counterface materials: CoCr, diamond-like carbon (DLC) coated CoCr, stainless steel and alumina (Al_2O_3). See Table IV for an overview of the tests.

The length of the wear tests ranged from two to five million cycles. The lengths of the BRM and CTPOD wear tests (Publications II and III; [50]), were three million cycles and the length of the ball-on-flat wear test (Publication I) was five million cycles. The HUT-3 test was a part of a longer test [49] in which different load cycles were used. The interval of lubricant change and polyethylene specimen weighing, was one million cycles in the earlier CTPOD tests [50] and half a million cycles in the later CTPOD tests (Publication III). In the other tests, the intervals were 300 000 cycles (BRM), 560 000 cycles (BOF) and one million cycles (HUT-3).

In each test, lubricant samples were taken between two and three million cycles to avoid the effect of running-in on wear. Hence, particles isolated from the lubricant represented steady-state wear conditions. From the lubricant, three samples of different volume were taken. The samples were digested with NaOH, neutralized with HCl and finally filtered with 0.05 μm Nucleopore

polycarbonate filters. Consequently, for each wear test, three filters with particles were obtained for scanning electron microscopy (SEM). Fourier transform infrared (FTIR) spectroscopy was used to identify the filtrates by comparing the spectra of the filtrates with spectra of the polyethylene components used in the tests.

The digestion procedure was needed because it was very difficult to separate the particles from the lubricant. It is known that the serum adheres strongly to the polyethylene, and cannot be directly filtered [22]. The digestion was done by adding 5N NaOH to samples of lubricant and subsequently letting the decomposition proceed in closed polytetrafluoroethylene vessels at 65°C for 6 h. The validity of the digestion was verified by checking with SEM that the morphology of particles of polyethylene powder (GUR 4150) was not changed by exposing the particles to a strong base at an elevated temperature for an extended period of time.

The morphologic features and the distribution of the particles on the filters was studied with scanning electron microscopy. With the objective of determining the size distribution using digital image analysis, the filter with as many individual particles as possible, distributed as evenly as possible, was selected for further study. Up to ten scanning electron micrographs, representing typical fields of view on the filters, were taken per selected filter.

The digital image analysis was done according to a semiautomatic procedure. Particles in the scanning electron micrographs were outlined and filled manually in an image processing program. Only separate particles were selected. Agglomerates and particles partially obscured by other particles were omitted. Then the micrograph was converted to a binary picture by thresholding [46]. Afterwards, the binary picture was processed by an image analysis program that counted the particles and provided a list of the area (A), the perimeter (p) and the major and minor diameter (d_{max}, d_{min}) of each particle. The following descriptors were calculated: equivalent circle diameter $ECD = \sqrt{(4A/\pi)}$, aspect ratio $AR = d_{max} / d_{min}$, roundness $R = (4A/(\pi d_{max}^2))$ and form factor $FF = 4\pi A/p^2$ (FF is a measure of roundness, but it is more sensitive than R to variations in roughness of the particle outline) were calculated [3]. The particles in the binary picture were categorized into rounded, elongated and irregular based on the following criteria. Rounded particles were those with $R > 0.7$, and elongated particles those with $AR > 2.7$. Particles that remained in the binary picture after the rounded and elongated particles had been removed, were categorized as irregular. Finally, the size distributions were visualized by preparing histograms and box-plots.

The image analysis process for particles isolated from a test with conventional polyethylene against a rough CoCr counterface in the CTPOD simulator (Publication III), is illustrated in Figure 4.

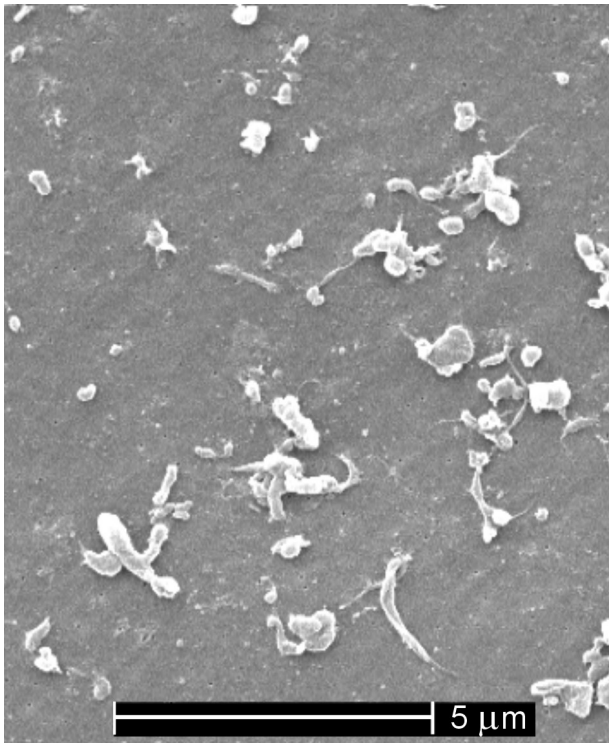

(a)

(b)

(c)

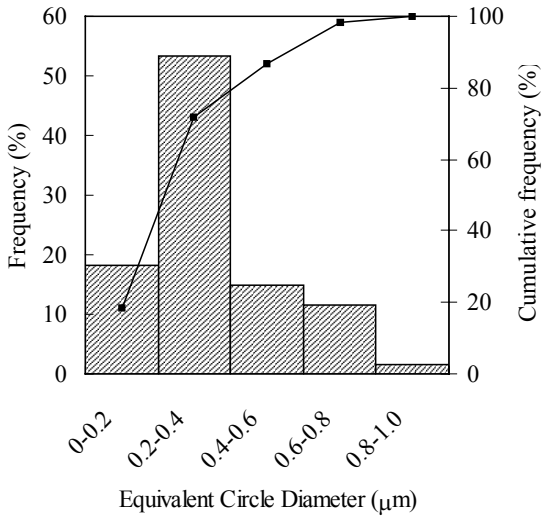

(d)

Figure 4. Example of image analysis of wear particles from test with conventional polyethylene against rough CoCr counterface. (a) Original 8 bit grayscale scanning electron micrograph. (b) Particles manually outlined and photo converted to black-and-white. (c) Example of particle classification, elongated particles with AR > 2.7 are shown in dark gray. (d) Size distribution of particles in (b).

Table IV. Wear tests from which lubricant samples for particle analyses were taken

Test	Simulator	Polyethylene		Counterface		Lubricant [b]		Wear factor	Ref. / Publ.
		Type [a]	Irradiated	Material	R_a (μm)	Type	Protein content (mg/ml)	k (mm^3/ Nm)	
1	CTPOD	GUR 4150	No	Al_2O_3	0.006	Bovine serum	73	1.6×10^{-6}	[50]
2	CTPOD	GUR 4150	No	SS	0.004	Bovine serum	73	2.3×10^{-6}	[50]
3	CTPOD	GUR 4150	No	SS	0.004	Albumin	40	1.9×10^{-6}	[50]
4	CTPOD	GUR 4150	No	SS	0.004	Globulin	10	2.4×10^{-6}	[50]
5	CTPOD	GUR 1020	γ	CoCr	0.022	Calf serum	21	1.9×10^{-6}	(III)
6	CTPOD	GUR 1020	γ	CoCr	0.24	Calf serum	21	1.8×10^{-5}	(III)
7	CTPOD	GUR 1050	Crosslinked	CoCr	0.014	Calf serum	21	1.6×10^{-9}	(III)
8	CTPOD	GUR 1050	Crosslinked	CoCr	0.22	Calf serum	21	1.7×10^{-6}	(III)
9	BRM	GUR 1050	γ	Al_2O_3	0.01	Calf serum	21	1.5×10^{-6}	(II)
10	BRM	GUR 1050	γ	CoCr	0.01	Calf serum	21	1.8×10^{-6}	(II)
11	BRM	GUR 1050	γ	DLC	0.01	Calf serum	21	1.8×10^{-6}	(II)
12	HUT-3	Himont 1900T	γ	CoCr	0.01	Bovine serum	24	1.7×10^{-6}	[49]
13	BOF	GUR 1050	No	CoCr	0.01	Calf serum	21	0.3×10^{-6}	(I)

SS = Stainless steel; DLC = Diamond like carbon coated CoCr

[a] Trade names of UHMWPE resins used to manufacture the polyethylene components

[b] Lubricant samples were taken between 2×10^6 and 3×10^6 cycles

Table V. Size and shape of polyethylene wear particles from tests described in Table IV

Test	Simulator	Polyethylene	Counterface		Lubricant	Area	*ECD*	Length	Aspect ratio	Roundness	*N*
		Irradiated	Material	Surface	Type	(μm^2)	(μm)	(μm)	(*AR*)	(*R*)	
1	CTPOD	No	Al_2O_3	Polished	Bovine serum	0.17± 0.20	0.42 ± 0.21	0.59 ± 0.43	1.88 ± 0.94	0.66 ± 0.23	159
2	CTPOD	No	SS	Polished	Bovine serum	0.13 ± 0.16	0.37 ± 0.18	0.60 ± 0.40	2.41 ± 1.46	0.52 ± 0.24	164
3	CTPOD	No	SS	Polished	Albumin	0.16 ± 0.23	0.38 ± 0.23	0.74 ± 0.73	2.86 ± 2.56	0.53 ± 0.31	102
4	CTPOD	No	SS	Polished	Globulin	0.14 ± 0.23	0.37 ± 0.22	0.53 ± 0.53	1.95 ± 0.97	0.62 ± 0.22	123
5	CTPOD	γ	CoCr	Polished	Calf serum	0.04 ± 0.04	0.21 ± 0.09	0.26 ± 0.14	1.69 ± 0.57	0.77 ± 0.21	340
6	CTPOD	γ	CoCr	Roughened	Calf serum	0.15 ± 0.24	0.37 ± 0.23	0.59 ± 0.51	2.05 ± 1.23	0.59 ± 0.24	149
7	CTPOD	Crosslinked	CoCr	Polished	Calf serum	0.01 ± 0.01	0.10 ± 0.04	0.12 ± 0.07	1.64 ± 0.44	0.88 ± 0.26	71
8	CTPOD	Crosslinked	CoCr	Roughened	Calf serum	0.16 ± 0.21	0.39 ± 0.22	0.52 ± 0.38	1.66 ± 0.54	0.68 ± 0.21	194
9	BRM	γ	Al_2O_3	Polished	Calf serum	0.08 ± 0.11	0.27 ± 0.15	0.41 ± 0.39	1.94 ± 1.57	0.61 ± 0.22	339
10	BRM	γ	CoCr	Polished	Calf serum	0.11 ± 0.11	0.33 ± 0.16	0.48 ± 0.35	1.79 ± 0.88	0.63 ± 0.21	281
11	BRM	γ	DLC	Polished	Calf serum	0.11 ± 0.10	0.33 ± 0.15	0.51 ± 0.40	1.95 ± 1.15	0.58 ± 0.20	209
12	HUT-3	γ	CoCr	Polished	Bovine serum	0.31 ± 0.89	0.45 ± 0.44	0.80 ± 1.26	2.20 ± 1.42	0.60 ± 0.27	151
13	BOF	No	CoCr	Polished	Calf serum	0.68 ± 1.86	0.69 ± 0.62	0.93 ± 0.92	1.70 ± 0.52	0.69 ± 0.23	199

SS = Stainless steel; DLC = Diamond like carbon coated CoCr

Sizing with a particle counter (Coulter N4MD) was done to compare SEM and digital image analysis with another method. The instrument analyzed particles within the diameter range from 0.003 μm to 3 μm using photon correlation spectroscopy. With photon correlation spectroscopy, one can obtain the size distribution of the entire sample of particles without the tedious work associated with scanning electron microscopy and image analysis. A sample of serum lubricant from the HUT-3 simulator was digested and analyzed. Unimodal and size distribution processor analyses were conducted. The unimodal analysis assumes a log normal size distribution, whereas the size distribution processor gives the size distribution without this assumption.

2.2 Slide track analysis

Slide tracks were chosen to illustrate the relative motion at the articulation surface of the hip. The tracks were produced by selecting marker points on the surface of the femoral head or the acetabular cup, and computing the motion of the points on the counterface during one cycle.

To compute the relative motion, two coordinate systems were placed at the mutual center of the cup and the head. The reference coordinate system XYZ was fixed relative to the cup. A moving coordinate system xyz was fixed relative to the head. The motion of a marker point was based on Euler rotations, see Figure 5 for an example of applying the rotation sequence FE→AA→IER. The axes of the moving coordinate system acted as rotation axes according to the rotation sequence determined for each simulation. The rotation angles applied to the axes were taken from a biomechanical study [31] or from published data of different simulator designs [5,10,21,25,30,47,49,57,59]. The FE, AA and IER angles for one cycle are shown in Publication V, Fig.1 and Publication VI, Fig.1.

The rotation sequence was determined according to the simulator design. The first rotation changes the orientation of both the remaining rotation axes of the simulator, relative to the reference coordinate system (the acetabular cup). The second rotation changes the orientation of the one remaining simulator axis relative to the cup. The third rotation does not change the orientation of any simulator axis relative to the cup. In two-axis simulator designs, the first step in determining the rotations was naturally omitted. The sequence for gait was FE→AA→IER, since the goniometer used by Johnston and Smidt [31] conformed to this sequence.

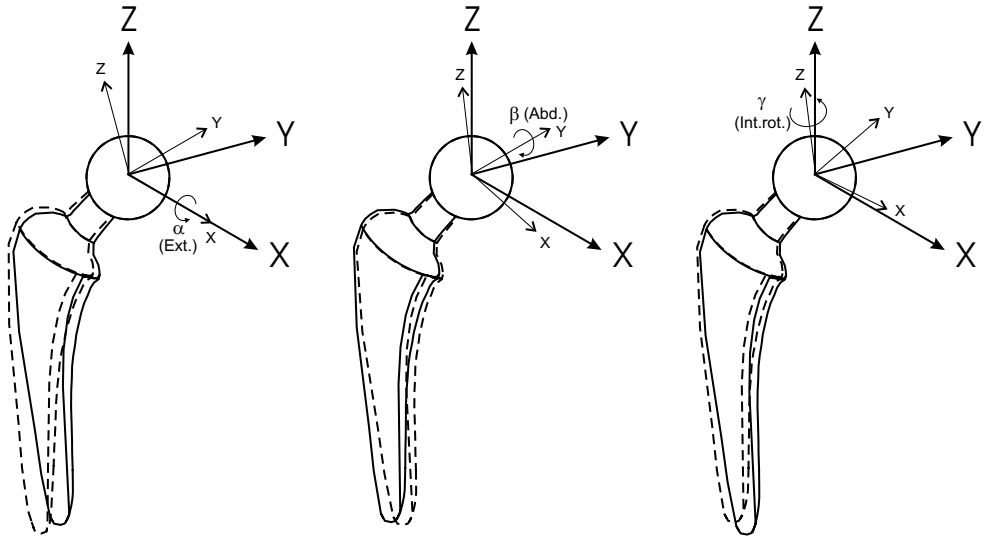

Figure 5. Euler rotations applied to the right hip. Sequence is FE→AA→IER, or α→β→γ. Note that in the computations, the positive signs of α, β and γ corresponded to extension, abduction and internal rotation respectively. The reference coordinate system *XYZ* was fixed relative to the cup and the moving coordinate system *xyz* was fixed relative to the head.

The computational procedure of determining the slide tracks is shown in Figure 3. The number of marker points was not restricted, and the location of the points could be freely selected. Theoretically, there are an infinite number of tracks, but too many tracks on one plot would result in a tangled image. Therefore, a limited number of points were chosen to produce an illustrative track pattern. For the computation, each waveform was discretized using 100 points per cycle. The computation is described in Appendix A of this thesis and in Appendix A of Publication V.

The computed slide tracks were verified both experimentally and by computing the tracks with alternative methods. Head tracks of the HUT-3 and HUT-BRM simulators were engraved with sharp pins of hardened steel, which were embedded in the acetabular cup (Publication V, Fig. 4). The pins were placed very carefully, to produce an accurate pattern. This was necessary in order to correctly place the corresponding marker points in the computational model. The simulators were driven for one cycle with load on, to produce the tracks. The lengths and locations of the force tracks were compared with the computed force tracks. In addition, the shapes of the individual tracks and the location of the overall track pattern were compared with the results of the computations. The effect of the shape of the rotation-prevention lever of the BRM simulators on the head tracks was studied both by engraving the track grooves, as explained above, and by letting a stationary pen draw tracks on the head while the simulator was driven without the cup (Publication VI, Fig. 5). The cup tracks of the BRM-simulator were checked by photographing the movement of head marker points with long exposure times.

Computational verifications included computing all tracks with two alternative methods in addition to the method of Euler rotations. The first method was to compute rotations about the fixed axes, but in reversed sequence. Both methods should yield the same end position [16]. The other method was to explicitly rotate the two other axes at the same time as the marker point was rotated about the first rotation axis (Publication V, Appendix A, Eq. A.5–A.10). In addition, the force track length of the BRM simulators was compared with the theoretical value of $2\pi r\sin 23° = 2.455r$.

3 RESULTS

3.1 Wear particle analysis

The particles on the filters were identified to be polyethylene. The peaks of the Fourier transform infrared spectrum of the filtrate matched the peaks of the reference spectrum collected from the tested polyethylene components (Publication IV, Fig. 1). The spectrum from the tested component shows stronger peaks because there is much more polyethylene present than on the filter.

The majority of the individual wear particles were rounded, and less than 1 μm in diameter. Fibrillar particles ranged from less than 1 μm to several micrometers in length. The width of these particles was generally only tenths of micrometers. These particles had the same shape as the fibrils that were found on polyethylene bearing surfaces. In addition, irregular particles were found that were in the same size range as the fibrils, but generally slightly shorter. Large, elongated particles (shreds) were occasionally detected, and they appeared to have smooth surface texture. The length of these particles ranged from 5 μm to 10 μm. Large, flakelike particles were detected in the samples from the knee wear simulator. The maximum dimension of the flakes ranged from 3 μm to 10 μm. Agglomerates were often seen in the micrographs. Agglomerates consisted of clusters of rounded particles, clumps of spherical particles, or patches of fibrous particles. In addition, the agglomerates were often combinations of various particle types (build-ups consisting of flakes, fibrils and rounded particles).

The results of the particle analyses for all the different wear simulation are listed in Table V. The range of the mean equivalent circle diameter was from 0.10 μm to 0.69 μm. A typical particle size distribution is shown in Fig. 8 of Publication IV. The majority of the particles were less than 1 μm in size, and large particles were considerably larger than particles on the average. The size distributions of different simulations were summarized in the equivalent circle diameter box plot in Fig. 9 of Publication IV. A similar box plot of the results in Publication III is shown in Figure 6.

The median *ECD*-value was less than 0.5 μm in all simulations. The size distribution of the particles from the ball-on-flat device was wider than the distributions of the particles from the other simulators, and the median *ECD*-value (0.48 μm) of the ball-on-flat distribution was larger than the median *ECD* values (0.10–0.32 μm) of the other distributions.

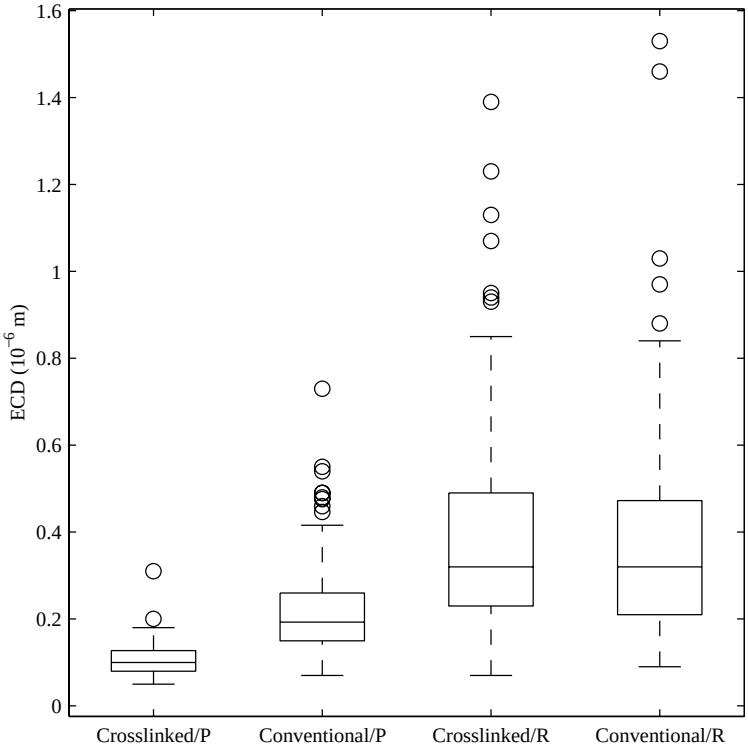

Figure 6. Size distributions of polyethylene wear particles from wear tests with conventional and crosslinked polyethylene against polished (P) and roughened (R) counterfaces (Publication III).

Large particles were likely to account for most of the wear volume if they were present in the distribution. The proportion of large particles in the debris was determined by computing the total wear particle area in different wear particle size ranges. In Publication IV, it was found that in the knee wear simulator, particles in the size range above 1 μm accounted for more than 70% of the total wear particle area (Publication IV, Fig. 10A). However, in the biaxial rocking motion simulator (CoCr ball and serum lubrication), large particles were not present. Particles less than 1 μm in size accounted for all of the total wear particle area (Publication IV, Fig. 10B).

The different tests suggest that some factors have little influence on the particle size distribution. Similar size distributions were obtained with different counterface materials, different

protein contents, whether normal sterilization irradiation (25–40 kGy) was used, and whether static or dynamic loading was used. Factors that strongly influenced the particle size distribution were counterface roughness, crosslinking and whether hip or knee simulation was conducted. However, tests 1–4 and 9–12 were not originally made with the purpose of evaluating the influence of counterface material, protein content, sterilization and loading on the *particle size distribution*. It was the *wear rate* that was being studied, and the particle size distributions were determined later to additionally verify that the wear conditions were similar to what has been found in clinical studies.

The Coulter particle counter produced the following results for a sample from the HUT-3 simulator. In the unimodal analysis, the mean particle diameter was 0.83 μm, and in the size distribution processor analysis it was 1.06 μm.

3.2 Slide track analysis

Different simulations could result in very different slide tracks (Publication V, Figs. 5, 6, 8). Slide track shapes included circular, elliptical, figure-of-eight, linear and various irregular shapes. The HUT-3 slide tracks were mostly elliptical, but tracks with very high aspect ratio and small track figures were also present. The gait slide tracks were mostly irregular ovals, having a characteristic thorn near the end of the gait cycle. The BRM slide tracks included a circle, egg and tear shapes, and figures of eight. The HUT-3 and gait simulations produced overall slide track patterns that were similar. The slide track pattern of the BRM simulation differed from the patterns of the other two simulations. In Publication VI, Figs. 3a-h show the slide track patterns of eight different simulators, computed according to the method presented in Publication V. Typical slide tracks of the AMTI and Leeds Mk I simulators were irregular ovals. Many of the slide tracks of the Munich simulator were leaf-shaped. The two axis simulators Durham Mk II and Leeds Mk II, had slide tracks that were linear, elliptical and figures of eight. The ProSim two-axis simulator had slide tracks with linear and multi-loop shapes with abrupt changes in the direction of sliding.

In general, the slide tracks on the head were similar, but not identical to slide tracks in the corresponding location on the cup. The greatest difference is that characteristic features (such as the thorn in many of the gait slide tracks) are in opposite directions with respect to the neutral position of the marker point (Publication V, Fig. 5b,c and Publication VI, Fig. 7). In the zero-offset lever BRM, the head and cup patterns are identical, but one is rotated 90° with respect to the other (Publication V, Fig. 8b,c).

In the BRM simulator, changing the type of rotation-prevention lever changed the slide track pattern. The lever with offset caused tilting and shift of tracks, compared with the zero-offset case

(Publication V, Figs. 9–10 and Publication VI, Fig. 5). The force track however, remained unchanged. In Publication VI, it was shown that a rotation-prevention lever with an offset introduced IER motion in the simulator, turning the BRM into a three-axis device and causing the change in slide track pattern. This experimental finding was reproduced in the computations by adding the IER motion to the BRM slide track simulation done previously (Publication VI, Fig. 6).

The length of the computed force track in the cases HUT-3, HUT-BRM and gait was 1.71*r*, 2.46*r* and 1.65*r* respectively (Publication V). For the simulators analyzed in Publication VI, the force track length varied from 1.41*r* to 1.75*r*. For the HUT-3 and BRM simulators, the shapes of the individual engraved tracks and the overall engraved track pattern agreed well with the computed tracks (Publication V, Figs. 6a, 7, 8a and 9). The lengths of the engraved force tracks of the HUT-3 and the BRM simulators were 24.2 mm and 34.6 mm, respectively for r = 14 mm. The lengths of the corresponding computed force tracks were 23.9 mm and 34.3 mm, differences being –1.2% and –0.9%, respectively. Both the computed and engraved force tracks had aspect ratios of 1 in the BRM simulator and 3.8 in the HUT-3 simulator.

The slide tracks visualize the direction of sliding and the extent of motion in different parts of the articulating surface. In addition, the variation in sliding speed along each track can be visualized. This was done in Figure 7, by dividing the cycle time into 100 equally spaced time steps and by plotting a dot on the tracks for each time step. The tracks were the force tracks of the HUT-3 and HUT-BRM simulators and the gait simulation. In the HUT-BRM simulator, the sliding speed is nearly constant during the motion cycle, while in the other cases, the sliding speed is slow at the extremes of the flexion-extension motion (upper and lower parts of the track figures), with a fast return movement in the second half of the cycle.

The direction of sliding at any moment during the motion cycle was given by the tangent to the slide track. A circular or elliptical slide track meant that the direction of sliding (and consequently the direction of the frictional shear stress) gradually changed 360° during one cycle. On a circular track, the rate of change of the direction of sliding was constant, assuming constant sliding speed. See, e.g., Fig. 7 and the BRM force track. When the track was elliptical, there were relatively small changes in the direction of sliding when the motion was roughly in the direction of the major axis of the ellipse, whereas the changes in the direction of sliding were large towards the ends of the ellipse. On tracks with a high aspect ratio, the motion was nearly reciprocating.

In the ball-on-flat device, the slide track was a narrow figure of eight located in the middle of the polyethylene disk, see Figure 8. The length of the track was 20.1 mm, height 10 mm and width 0.4 mm.

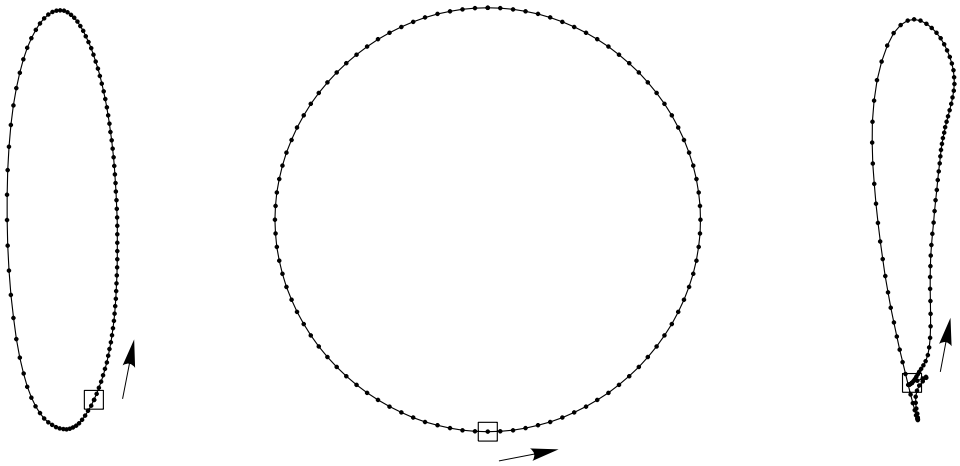

Figure 7. Slide tracks of the point of joint contact resultant force (force tracks) for the HUT-3, BRM and gait simulations. The small box indicates location of heel strike and the arrow indicates the direction of sliding. One dot is plotted for each equally spaced time step. A decrease in the density of dots along the track indicates an increase in the sliding speed.

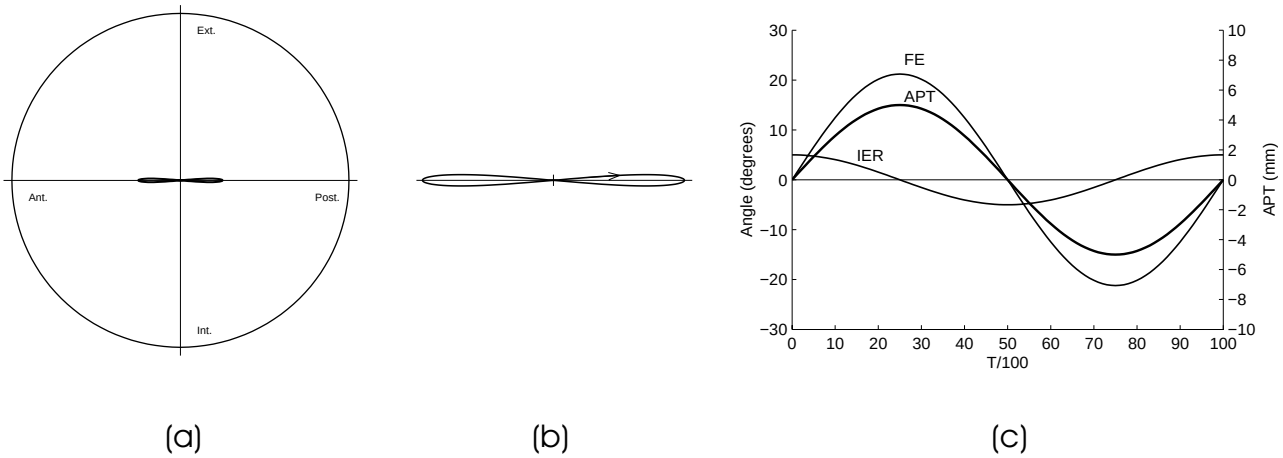

Figure 8. Slide track and motion waveforms of Ball-on-flat simulator. (a) Slide track on the 40 mm diameter polyethylene disk is shown. The length of the track was 20.1 mm. (b) Magnified view of the slide track. The anterior-posterior extent of the track was 10 mm and the internal-external extent was 0.4 mm. Arrow shows direction of sliding. (c) Waveforms of flexion-extension (FE), internal-external rotation (IER) and anterior-posterior translation (APT).

4 DISCUSSION

4.1 General

In this thesis, wear simulations according to four different principles were validated. The principles were flat-on-flat contact and two-axis motion, ball-in-socket contact and two-axis motion, ball-in-socket contact and simulated three-axis walking motion, and ball-on-flat contact and three-axis motion. The last principle, involving non-conforming contact, represented knee wear simulation, while the others represented hip wear simulation. The principles were implemented by four simulators (CTPOD, HUT-BRM, HUT-3 and BOF) designed by Dr. Saikko at Helsinki University of Technology. Two different validation approaches, wear particle analysis and computational analysis of relative motion, were applied. These approaches had not previously been applied in wear validation of the simulators. The approaches were linked in that, especially for polyethylene, multidirectional motion is a requirement for producing wear particles of a size and shape corresponding to clinical findings [60]. For the BRM simulator, validations have previously been done for the design with an offset rotation prevention lever [37,60,64]. In this work, the HUT-BRM with a zero-offset lever was validated.

In prosthetic joints with polyethylene articulating against a hard counterface, the outcome of the wear simulation (for a given contact geometry) is mainly influenced by the following factors:

(i) The polyethylene itself, its type and state. The variations in type, depending on the molecular weight, whether calcium stearate was used during manufacturing, and the manufacturing process itself (ram extrusion, compression molded sheet or direct compression molding into near net shape), may not influence the outcome of the wear test as much as the state [6,34,39,III]. The state varies depending on whether the polyethylene was non-irradiated, sterilized by gamma-irradiation, or crosslinked.

(ii) The counterface. The surface roughness is crucial with respect to wear, and the hardness is important, because a harder material is more resistant to scratching [18,38,III].

(iii) Presence of abrasive particles. Hard particles, such as fragments of bone or polymethylmethacrylate (PMMA, bone cement), can cause roughening of the counterface [4] and additionally abrasion of the polyethylene, either directly [37], or by adhering to the counterface [66].

(iv) Lubrication. In studies on polyethylene wear, water lubrication has been shown to underestimate the wear, and to produce wear particles that are too large compared to what has been seen in clinical studies [61]. Serum lubrication has been shown to produce wear that agrees with clinical findings [37,60,61]. The proteins albumin and gamma-globulin have been shown to be the most important constituents with respect to wear in the serum lubricants [1].

(v) The relative motion. Linear, reciprocating motion has been shown to underestimate the wear, while exaggerating the effect of counterface roughness on wear [64]. In the hip joint, the direction of sliding changes continually during walking motion. In the computational simulation of gait and three-axis simulators such as HUT-3 and Munich, the continually changing direction of sliding was manifested by open force track figures (Publication V, Figs. 6–7 and Publication VI, Fig. 3c). In the knee joint, the relative motion is closer to reciprocation, but due to IER, the direction of sliding will nevertheless change more than twice during one cycle (Fig. 8).

(vi) Loading. During walking, the loading is naturally dynamic. Simulator tests with static loading have, however, been shown to produce wear factors that agree well with wear factors based on clinical wear measurements [50,II].

In a simple model of the simulation process (Figure 9), the wear simulation factors can be categorized as input and simulation variables. The worn components and the wear debris are output. The output is studied by assessing the visual and microscopic appearance of the components, by measuring the wear, and by analyzing the size and shape of the wear debris. Energy is needed to produce the relative motion between the components. Part of the energy brought to the process is dissipated as frictional heat. The simulation variables correspond to factors iii)–vi). The type of relative motion, the lubricant and the loading must be adjusted until the wear results are in agreement with clinical results for the given material combination. It could even be argued that abrasive particles should be added to the lubricant to obtain realistic wear rates. Such an addition of hard particles would, however, require a specification of the type of particles and their concentration.

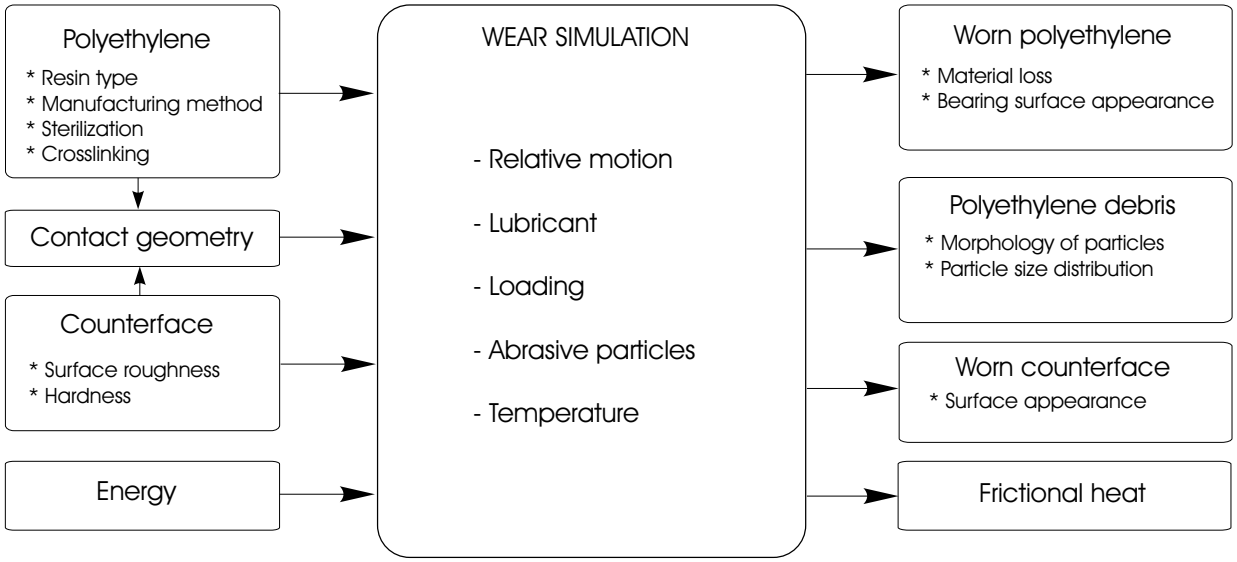

Figure 9. Simple process model of polyethylene wear simulation. The material pair, forming the contact geometry, and energy to produce the relative motion are input. The worn components and the wear debris are output. Some of the input energy is transformed to frictional heat. On the left, properties of the polyethylene and the counterface are listed. On the right, there are properties that must be checked against clinical criteria, in order to validate the wear simulation. The simulation variables are listed in the middle. In the development of the wear simulation process, these variables must be correctly set to produce clinically relevant output with given input materials.

In judging whether the outcome of the wear simulation has been clinically relevant, the basic criteria are [1,14,28,37,50,53,64]:

(a) The polyethylene bearing surface is burnished. Microscopically, the burnished surface contains ripples, patches of fringes, cracks and scratches (Fig. 10; Publication I, Fig. 4; Publication II, Fig. 4).

(b) The counterface is free from polyethylene transfer film.

(c) Scratches on the counterface, if present, are multidirectional.

(d) The wear factor is of the order of 1×10^{-6} mm^3/Nm for conventional polyethylene.

(e) The majority of the wear particles are in the 0.1–1 μm size range.

In addition, the correct wear resistance ranking should be reproduced for materials with documented clinical wear rates [64].

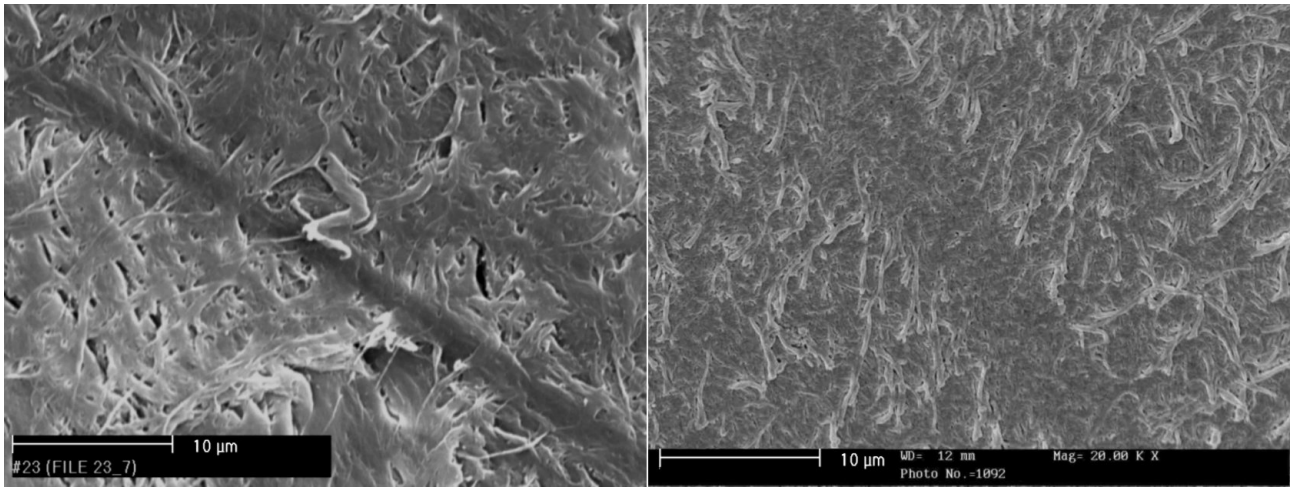

(a) (b)

Figure 10. Micrographs of conventional polyethylene bearing surface of acetabular cups worn against CoCr counterfaces. (a) Cup worn in vivo for 104 months. (b) Cup worn in simulator (HUT-BRM) for three million cycles. The surfaces contain a scratch, surface cracks and fibrillar features (fringes).

Factors (iv) and (v) above, provide the means for fulfilling the criteria (a)–(e). The relative motion must be arranged so that the direction of sliding changes continually during the cyclic motion, and serum or a protein containing lubricant based on albumin or globulin must be used. In fact, continually changing direction of sliding is a design requirement for simulators to be used for assessing polyethylene wear [62].

In all wear simulations reported in this thesis, the basic criteria (a)–(d) were fulfilled. The polyethylene bearing surface was burnished and the counterface was free from polyethylene transfer film. In laboratory tests, the counterface is generally flawless since abrasive particles are not present, unless they are added on purpose as part of the test. In Publication III however, the counterfaces were deliberately roughened with multidirectional scratches to study the effect of surface roughness on wear. For conventional polyethylene against polished counterfaces, the wear factors ranged from 0.3–2.4 $\times$ 10^{-6} mm^3/Nm, satisfying criteria (d).

Note that all the criteria (a)–(e) must be satisfied to fully validate the wear simulation. It is possible to achieve a wear factor in accordance with (d) without multidirectional motion. Then however, other factors mentioned in (i)–(vi) must be changed. For example, valid polyethylene wear factors can be achieved with an ordinary pin-on-disk device, by increasing the counterface surface roughness and using water lubrication [9]. Currently, wear simulation with multidirectional motion and serum lubrication (protein content in the range 20–35 mg/ml) represent proven procedure [64,65]. Departing from proven procedure must be done with great caution. The risks of

producing erroneous wear results are greatest when new materials and designs are introduced, since clinical reference values are not yet available.

This thesis focuses on the measurement of the size and shape of the polyethylene debris, and the computational analysis of relative motion. The debris is one of the output variables and the relative motion is one of the intrinsic variables of the simulation process. For the simulators dealt with in this study, thorough investigations of neither variable have previously been published.

4.2 Wear particle analysis

In studies of particles collected in connection with hip revisions, the particles have generally been found to be less than 1 μm in size [13,14,37,55]. The average particle size from total knee replacements has been found to be larger and to range from 0.5 μm to 1.7 μm [53,56]. The average size of particles isolated from the lubricants of different simulators was within these size ranges. In all tests, the particle size ranged from 0.1–5.2 μm and the average particle size was less than 0.7 μm. In the hip wear simulations practically all particles were smaller than 1 μm, only some outliers were larger (Fig. 6 and Publication IV, Fig. 9). In the knee wear simulation, the particle size distribution extended beyond 1 μm, but still the majority of the particles were smaller. These results show that criterion (e) was satisfied. As explained in the Introduction, it is extremely important that the majority of the particles produced in the wear simulations were smaller than 1 μm. These small particles are likely to trigger off the immune defense system reactions that can lead to osteolysis and eventually to implant loosening and reoperation.

In clinical studies [13,14,37,53,56], the particles have been found to be rounded, elongated or flake-like. The rounded particles are smaller granules and larger beads. Elongated particles are short fibrils and longer shreds. Fibrils often have a rounded head at one end. Clusters of particles (agglomerates) are also found [56]. In Publications I–IV, particles isolated from the simulator lubricants were found to have essentially the same shape as the particles found in clinical studies. Most of the separate particles were rounded or fibrillar. Shreds were less common. A large proportion of the particles were neither rounded, nor elongated and were simply classified as irregular. For the knee wear simulator, the average particle size was larger than for the hip simulators. Debris from the knee wear simulator contained large flake-like particles. In a hip wear simulator study by McKellop et al. [37], predominantly rounded particles were generated. The elongated particles were mostly fibrils. Few shreds were found. In a study by Wang et al. [60], the particles from the hip wear simulator were fibrillar or equiaxed. The particles from the knee wear simulator were mostly fibrillar, but large flake-like particles were also present. Consequently, the

shape of polyethylene particles reported in Publications I–IV corresponded well with the shape of particles reported in other simulator studies. Because the studied simulators (CTPOD, HUT-BRM, HUT-3 and BOF) produced polyethylene particles of size and shape comparable to what has been found in periprosthetic tissues, it can be concluded that the same wear mechanisms act in the simulators as in the artificial joints in vivo.

The basic wear mechanisms of polymers are abrasive, adhesive and fatigue wear [18,35]. Abrasion is caused by hard third-body particles, trapped between the articulating surfaces, or by asperities of the hard counterface. Adhesion involves bonding of solids together through attractive molecular forces, acting at local spots of contact. The polymer material near the adhesive bond undergoes severe straining until the junction fails, and the material is either transferred to the counterface, or released as a wear particle [18,64]. Fatigue wear is related to cyclic variations in compressive and shear stresses of polymer asperities (microfatigue), which leads to gradual buildup of subsurface strains until fracture occurs, and wear particles are detached [15,64]. In non-conforming contacts, such as in the knee joint, fatigue is not limited to the polymer asperity level, because the contact stress field moves according to the FE motion (macrofatigue).

In addition to the basic wear mechanisms above, Wang et al. [60,62,63] have proposed a mechanism which takes into account the molecular structure of polyethylene. Under the influence of the interfacial shear stresses, the polymer chains near the surface will become aligned in the direction of sliding. Due to loading during walking, the highest interfacial shear stresses occur in the FE direction, and the surface polymer chains will mainly become oriented in this principal direction. The strength of the polymer surface in the transverse direction is lower than in the principal direction, and transverse shear stresses (due to multidirectional sliding) will lead to a molecular splitting wear mechanism in which wear particles are produced due to rupture of fibers between the oriented polymer chains.

Table VI presents an overview of bearing surface features and wear particle morphologies seen in the wear tests (Publications I–IV) with conventional polyethylene against polished counterfaces. In the following, the observations are related to different wear mechanisms.

Adhesive wear was suggested by the presence of smeared fringes on the wear surface (Publication II, Fig. 4), while the multidirectional scratches (due to occasional hard particles) and torn fringes (produced with rough counterfaces) could be related to abrasive wear (Publication II, Fig. 4 and Ref. [52], Fig. 2b). The surface microcracks (Publication II, Fig. 4) represented fatigue damage. The ripples (Publication I, Fig. 4) were probably caused by repeated deformation of surface asperities, resulting in strain accumulation. This could happen through a stick-slip type of mechanism. Wear simulation of conventional polyethylene against polished counterfaces, in the

clean conditions in the laboratory, suggested that the adhesive and fatigue wear mechanisms dominated. It was most likely that these two mechanisms operated simultaneously, because micrographs often revealed fringes on a surface containing microcracks (Publication III, Fig. 4). According to Wang et al. [60], the inter-fiber splitting wear initiates with the formation of microcracks between fibers, eventually producing fiber-like wear debris. It could, indeed, be possible that inter-fiber splitting weakens the polyethylene matrix, so that the adhesive and fatigue wear mechanisms can become effective. Macroscopically, the polyethylene bearing surface looked burnished, and fringes and ripples were not seen. Actually, the glossy appearance of the bearing surface, and the multidirectional motion, suggest the wear conditions of a lapping or polishing process, albeit without the presence of purposely added fine abrasives. Macroscopic cracks and starting delamination were seen only in the ball-on-flat knee wear tests, with irradiated and O_2-aged disks (Publication I).

Table VI. Bearing surface features and polyethylene wear particles identified in tests with conventional polyethylene against polished counterfaces (R_a = 0.01 μm) in serum lubrication.

Simulation	Bearing surface [(a)]	Wear particles	
	Features	Shapes	Size ranges (μm)
Hip (CTPOD,BRM,HUT-3)	Fringes, cracks (microscopic), ripples, scratches	Rounded	0.1–1.6
		Irregular	0.2–2.9
		Fibrils	0.1–5.0
		Shreds	5–10
Knee (BOF)	Ripples, cracks (macroscopic), delamination	Rounded	0.1–0.9
		Irregular	0.3–5.2
		Flakes	3–10

[(a)] Macroscopically, the bearing surfaces were burnished

The fibrillar wear particles were likely to be the result of a combination of adhesive and fatigue wear mechanisms. Polyethylene that momentarily adheres to the counterface would get partially pulled out in the form of fibrils, attached to the matrix by one end. Additionally, fibrils could be produced by molecular splitting. In any case, the loose ends of the fibrils would be shifted around by the frictional shear stresses that continually change their direction. Eventually the fibrils would detach due to fatigue, forming wear particles. The rounded wear particles could be formed directly by the release of rounded substructures of the polyethylene matrix, due to fatigue [37]. This

assumption is supported by the fact that unprocessed polyethylene powder particles have been shown to consist of spheres smaller than 1 μm, which are interconnected with nanometer-sized fibrils [42]. Alternatively, the rounded particles could be formed indirectly, by the reduction of larger particles (e.g., fibrils with rounded ends) by the motion of the joint [14]. Large particles can be formed by third-body abrasion (shreds) or, in the case of knee wear simulation, by macroscopic fatigue and delamination (flakes). A comminution process is also a likely explanation for the presence of small (< 1 μm), irregular wear particles.

The wear resistance of polyethylene was significantly improved by crosslinking. The wear factors of conventional and crosslinked polyethylene worn against polished counterfaces in the CTPOD simulator were 2×10^{-6} mm^3/Nm and 2×10^{-9} mm^3/Nm, respectively (Publication III). Crosslinking will inhibit the molecular reorientation that would otherwise be caused by the shear stresses at the polyethylene surface. Consequently, it is likely that the molecular splitting wear mechanism becomes inactive. This was evidenced by the fact that few fibrils were seen in micrographs of the bearing surfaces and of the wear particles. Apart from molecular splitting, the same wear mechanisms (adhesive, fatigue and abrasion) appear to prevail as with conventional polyethylene under the same wear conditions. This assumption was supported by the observations that the bearing surfaces of crosslinked polyethylene were burnished and in micrographs showed fine ripples and microscopic cracks, together with multidirectional scratches. Against polished counterfaces, these wear mechanisms produced very small (average *ECD* = 0.10 μm), predominantly rounded, wear particles (Publication III, Fig. 5c and [52], Fig. 3c).

The effects of different factors on the polyethylene wear particle size distribution, such as the counterface material and surface roughness, the polyethylene type and the lubricant protein content, were treated in Publications III and IV. One of the observations made in Publication IV was that the particle size distribution was not influenced much by the material of the polished counterface. The average particle sizes (*ECD*) obtained for alumina, CoCr and DLC-coated CoCr counterfaces were 0.27 μm, 0.33 μm and 0.33 μm, respectively. This agreed with a study by Campbell et al. [14] on particles isolated from 25 hip replacements, reporting that factors that affect the polyethylene wear rate (head material, implant design, type of fixation, patient activity) have little influence on the size and shape of the polyethylene wear particles. The lubricant protein content is known to affect the *wear rate* in such a way that the highest rates are obtained in the range 10–40 mg/ml [51,64]. However, in Publication IV the effect of the lubricant protein content on the *particle size distribution* was found to be weak. In the CTPOD tests with polished stainless steel against unirradiated polyethylene, three different lubricants (Bovine serum, albumin and globulin) were used. The corresponding *ECD*-values of the wear particles and the protein contents were 0.37 μm

(73 mg/ml), 0.38 μm (40 mg/ml) and 0.37 μm (10 mg/ml), see Tables IV and V, Tests 2–4. It appears that the variation in protein content in these tests did not cause big enough changes in the lubrication conditions to affect the particle size distribution. In Publication III it was shown that against a polished counterface, the size distribution of the particles was different from that obtained against a rough counterface. Additionally, the size distributions for conventional and crosslinked polyethylene were different, see Fig. 6. The average *ECD*-values for conventional polyethylene were 0.21 μm against polished (R_a = 0.022 μm) and 0.37 μm against rough (R_a = 0.24 μm) counterfaces. The corresponding *ECD*-values for crosslinked polyethylene were 0.10 μm (R_a = 0.014 μm) and 0.39 μm (R_a = 0.22 μm). Changing from conventional polyethylene to the much more wear resistant crosslinked polyethylene was not reflected in the particle size distribution when the counterface was rough, but only when the counterface was polished. The knee wear simulation (BOF) produced wear particles that were larger on the average than those produced in the hip wear simulations (CTPOD, BRM, HUT-3). The average *ECD*-value of the particles from the knee wear simulation was 0.69 μm, while the average *ECD*-value was less than or equal to 0.45 μm for the hip wear simulations. It can be concluded that significant changes in the wear conditions were reflected in the particle size distribution, while smaller changes, such as shifting to a new counterface material (with the same surface roughness), did not change the distribution much.

In the tests with the crosslinked polyethylene against a rough counterface, the wear factor was an order of magnitude lower than for the conventional polyethylene, but the particle size distribution was the same. This suggests that a substantially lower number of particles were generated with the crosslinked polyethylene than with the conventional polyethylene. For crosslinked polyethylene worn against a polished counterface, the average wear particle size (0.1 μm) was below the biologically active size range. It can therefore be argued that the particles would be less harmful with respect to implant loosening. Because production of cytokines involved in the osteolysis process is stimulated by particles in the size range 0.2–8 μm, the use of crosslinked polyethylene could increase the life of prosthetic joints.

The particle sizing used in this research was chosen because it was the current state-of-the-art method. The approach taken in Publications I–IV was similar to the methods adopted in many important studies of polyethylene wear particles retrieved from periprosthetic tissues [13,33,55,56]. However, the protocol originally developed for tissue samples was simplified by omitting the centrifugation, because in the present research, the particles were isolated from simulator lubricants or synovial fluid. Other studies have confirmed that centrifugation can be omitted, whether base digestion [41] or acid digestion [54] has been used.

Several factors may influence the accuracy of the particle sizing method. Therefore, the following measures were taken to ascertain that a correct particle size distribution was obtained. That digestion and filtering did not alter the morphology of the wear particles, was verified by isolating polyethylene powder (GUR 4150) particles from serum lubricant using the same protocol as for wear particles. The morphology of untreated powder particles and isolated powder particles was found to be the same upon inspection with SEM. Filtering was done with 0.05 μm pore size polycarbonate filters to catch even the smallest polyethylene particles. Recent studies [54] have shown that with 0.2 μm pore size, a substantial number of wear particles will pass freely through the filter compared to the 0.05 μm pore size, which results in an overestimation of the mean and median particle size. For each filter that was selected for imaging with SEM, five to ten different micrographs of typical fields of view were taken. A low concentration of particles on the filters necessitated taking more micrographs. For example, of the filters with particles from the tests with conventional and crosslinked polyethylene against a polished counterface, five and ten micrographs were taken, respectively.

In the image analysis, the agglomerates were omitted. This was done because it was not possible to accurately determine the shape and number of particles below the topmost particles. Nevertheless, since most agglomerates consisted of clusters of particles with the same morphologic features that the separate particles on the filter had, it was considered that omitting the agglomerates would not significantly change the particle size distribution. In order to avoid the adverse effects of automatic thresholding of the 8-bit grayscale micrographs, the particles were manually painted in an image processing program prior to transferring the micrographs to an image analysis program to count the particles and determine their sizes. In thresholding, pixels with an intensity value below the threshold value were set to black, and the rest were set to white. In SEM imaging, particle edges that rose steeply from the background were easily detected on the screen and they got a high intensity value in the micrograph. Particle edges that rose at a shallow gradient from the background were difficult to detect and they got an intensity value close to that of the background in the micrograph. In fact, only sudden changes in height got high intensity values and all flat surfaces got low intensity values in the micrographs, even if they were located on a particle. As a consequence, the area of an individual particle could vary considerably when the threshold value was varied, and it was not possible to find a threshold value that would correctly outline all particles in the micrograph. A threshold that produced the right outline of some of the particles, could underestimate the area of other particles. Another problem was that automatic thresholding could cause particles to merge or divide. Consequently large, artificial particles can be created in areas of closely spaced particles, or numerous very small artificial particles can be created from a few large

particles. Fully automatic image analysis requires a starting image with good contrast between particles and background, and with separate particles evenly distributed over the image area. Whether this can be achieved, depends on the concentration of particles in the samples of lubricant, and on the filtering process.

The samples from the HUT-3 simulator showed that the mean particle size obtained with the photon correlation spectroscopy particle counter was larger (0.83 μm unimodal, 1.06 μm size distribution processor) than the mean size obtained using scanning electron microscopy and image analysis (0.45 μm). A likely explanation for the difference was that the particle counter included agglomerates in the sizing [13], whereas in the image analysis, the agglomerates were not taken into account. Comparable results were obtained for debris isolated from tissue samples taken at hip revision surgery, with a particle analyzer based on the low angle laser light scattering [24], which is a similar sizing method. Consequently, the debris from the HUT-3 simulator was in the same size range as debris collected at hip revisions, also when assessed by a technique other than scanning electron microscopy and image analysis. In addition, changing the sizing technique did not change the fact that the wear particles were found to be in the biologically active size range of 0.2–8 μm.

4.3 Slide track analysis

The slide track computations made it possible to visualize the relative motion at the articulation and to qualitatively compare different simulator designs with each other and with the slide track pattern pertaining to walking motion. But the software could additionally offer a basis for quantitative analysis of sliding distances, sliding speeds, the integral $\int Ldx$ (used in computing the wear factor k), and the changing direction of sliding during the motion cycle. This is needed in the development of an improved wear factor, which takes into account the variation in loading and motion on the whole contact surface of different wear simulators.

In Publication V, computed slide tracks for hip simulators were presented for the first time together with their verifications. The tracks were verified by checking that grooves engraved on the femoral heads in two different simulators were identical to the computed slide tracks. Additional verifications were done by drawing slide tracks on various locations of the head with a stationary drawing pen, while the simulator was run without the cup. The length and angular extent of slide tracks were verified by comparing computed values with values measured from the engraved grooves. For example, the diameter of the BRM force track on a 28 mm diameter head was measured to be 11 mm, implying a force track length of 11π mm = 34.6 mm. The computed track length was 34.3 mm, which was 0.9% less than the measured value. Theoretically, the force track

length should be $2\pi r\sin 23° = 2.46r = 34.4$ mm. The computed value is 0.3% less than the theoretical value and the measured value is 0.6% greater. The small difference between the measured value and the theoretical value may well be due to the engraving process, in which high loads were acting on the hardened steel pins during the engraving cycle. If the wear is considered to be directly proportional to the sliding distance, using either the computed or the engraved tracks would cause less than 1% error in wear compared to the theoretical value. This gives great confidence in both the slide track computations and their verifications.

Slide tracks were computed from the gait waveforms [31] with the same method of computation that was verified with the HUT-BRM and HUT-3 simulators, which makes the gait slide track pattern a reference case to which simulator slide track patterns can be compared. Note however, that the gait waveforms were measured with subjects having a natural hip joint, not a prosthetic joint. In addition, the gait waveforms may contain some inaccuracies (due to slipping of the goniometer attachment to the soft tissues of the test subject, and differences in anatomical and goniometer axes, especially the AA and IER axes), as noted in Publication V and the study by Ramamurti et al. [43]. Nevertheless, it can be considered that since the essential features of walking motion inevitably are captured in the gait waveforms, they can be used to compute the reference slide track pattern. Similar slide track patterns were produced only by some of the three-axis simulators (HUT-3, Munich, Leeds Mk I, ISO/DIS 14242-1) (Publications V and VI).

Publication V is the first study that the author knows of, to present the correct (experimentally verified) slide track pattern of the most popular hip wear simulator, the BRM. Additionally, it was shown that changing the shape of the rotation-prevention lever changed the slide track pattern. In Publication VI this was shown to be due to the addition of IER motion. The influence of the shape of the rotation-prevention lever can be seen in Figs. 9 and 10 in Publication V, and Figs. 5 and 6 in Publication VI.

The motion waveforms used in the HUT-3 simulator were idealizations of the gait waveforms measured by Johnston and Smidt [31]. This explains why the overall slide track patterns for the gait and HUT-3 computations resembled each other. Many of the gait tracks had a thorn towards the end of the motion cycle because of the sudden changes in FE and IER. It is unlikely that a simulator would need to duplicate these sudden changes that last only for a short period of the total motion cycle, since simulators with smooth circular force tracks (BRM, CTPOD) have been shown to produce realistic polyethylene wear.

The aspect ratio of the force track can, however, influence the wear rate. Under similar wear conditions (28 mm diameter polished CoCr head, serum lubricant and similar load) the wear rate produced by the BRM simulator was found to be twice that produced by the HUT-3 simulator [49].

In the BRM, the aspect ratio was 1 (circular force track), whereas in the HUT-3, it was 3.8 (elliptical force track). The elliptical shape is closer to reciprocating motion, which is known to result in minimal wear [48,62]. Hip simulators are usually designed so that the FE motion dominates in the high pressure region of the contact. The resultant contact load resides far away from both the FE and the AA axes, but near the IER axis. Because the FE motion has the largest amplitude, it will have a larger influence on the force track shape than the AA motion. The influence of the IER motion is smaller than the influence of the FE and AA motions, because the distance from the IER axis is small. Consequently, in the high pressure region of three-axis simulators, the major and minor dimensions of the slide tracks were determined mainly by FE and AA, which resulted in roughly elliptical slide tracks. Note that it was not only the magnitude of the rotation angle that influenced the displacement of the marker point on the spherical surface. The distances from the marker point to the rotation axes also influenced the displacements. This explains why the influence of IER on the shape of the force track was smaller than the influence of AA, even if the amplitudes of both motions were nearly equal. In the two-axis simulators with the IER→FE sequence, the motion in the region near the force track is essentially reciprocating with IER rotation superimposed, as evidenced by linear head tracks and high aspect ratio cup tracks in the Mk II simulators (Publication VI, Figs. 3f and 3g). In the high pressure region of the BRM simulators, the FE motion did not dominate over the AA motion, resulting in tracks with aspect ratios close to one.

Computed slide tracks of the BRM simulator published by another research group [44] were found to be incorrect, since the tracks contradicted the experimental verifications of the slide tracks of the BRM simulator both with and without an offset lever (Publications V and VI). The present method of computation, based on Euler angles, was shown to produce the correct slide tracks for both types of the BRM simulator. The slide track pattern computed by the other research group [43, Fig. 3] for the motion waveforms presented by Johnston and Smidt [31], disagrees with the pattern presented in Publication V, Fig. 5c. The differences are apparently due to the use of different principles of rotation and flattening. It is believed that the gait slide track patterns presented in Publication V correctly correspond to the gait waveforms, since the computational procedure was verified with the HUT-BRM and HUT-3 simulators, and an Euler sequence corresponding to how the electrogoniometer in the study by Johnston and Smidt recorded the motion waveforms was used.

It should be noted that the approach presented in this thesis is not just a slight modification of a method presented earlier [43] to correct minor mistakes. Rather, it is a new systematic method of determining the relative motion of marker points at the articulating surface of the hip joint. First, the

Euler sequence is determined (Section 2.2 and Publication V), and then the rotation angles are applied in accordance with the sequence. The rotations are not applied about the axes of a fixed coordinate system, as was done in previous studies [43, pp.847-848]. The rotations *could* be applied in the inverted order about fixed axes [16], but even then the correct sequence must be determined first. In a previous study [44], the BRM slide tracks were computed with a method different from the method presented by the same research group earlier [43]. The slide track pattern was, however, incorrect (Ref [44], Fig. 3C), as shown by the computations and experimental verifications in Figs. 8 and 9 in Publication V. In the present research, the BRM was not treated as a separate case. The same computational procedure was used as for the HUT-3 simulator and the gait waveforms.

Furthermore, it should be noted, that the slide track pattern is not just a question of visualization. A correct pattern verifies that the correct relative motion is produced all over the articulating surface, which is needed if the motion computation procedure is to be used as a basis for mathematical wear simulation.

In the method presented in Publication V, each track point was computed by applying repeatedly the rotation angles corresponding to each time step to the marker point in the neutral position. This was done to avoid accumulation of numerical errors that can produce an artificial discontinuity during the last time step of the cycle. This kind of error could be 'hidden' by choosing very few track points (using e.g. 10 instead of 100 time steps), which would result in a crude and jagged track, so that the last displacement would not appear to differ very much from the other displacements. Computing the displacements from a base point in the neutral position (and not from the previous track point) is thought to be a solution, which has not been used earlier in slide track computations.

Another new solution was that the flattening of each slide track was done 'locally' with respect to the neutral position of the marker point. As a result, the distortion introduced by flattening the tracks was kept to a minimum. A 'global' flattening of all tracks with respect to the pole point of the articulating surface, exaggerated the circumferential dimensions of the tracks near the equator and was therefore discarded.

Previous studies [43,44] have presented slide tracks traced by marker points on the head, i.e., cup tracks. In the present research, cup tracks were drawn to facilitate comparison with earlier work, and to show the placement of the force track in cases where the simulator load was fixed with respect to the femoral head. In Publications V and VI, head tracks were presented for the first time. The head tracks show how points on the polyethylene slide against the counterface. Head tracks make it possible to correctly compute the sliding distances of differential area elements of polyethylene. The sliding of an area element of the acetabular cup can be compared to the sliding of

the polyethylene pin against the counterface disk in the CTPOD simulator. When determining the wear factor for simulators with the load fixed with respect to the cup, the head force track must be used in computing the integral $\int L\mathrm{d}x$. Because the head and cup track patterns were similar, both could be used for qualitatively assessing the relative motion at the articulation. Distinct features of the head and cup tracks would, however, be located in opposite parts of the area where the track figures resided, see e.g. Publication V, Fig. 5 or Publication VI, Figs. 3c and 7).

There were considerable differences in the computed slide tracks of different simulators. At present, it is only possible to qualitatively compare the simulators, e.g., by noting that under similar wear conditions, a higher force track aspect ratio implies less wear [49]. Quantifying the relationship between the slide track pattern and wear would require wear tests with the same type of specimens, lubricant and loading. Unfortunately, the published wear test reports cannot be used for finding such a relationship, because they differ from each other regarding the materials, the type and dilution of serum, etc. Therefore, it would be feasible to conduct tests under similar wear conditions, and only vary the slide track pattern. The method presented in Publication V can then be used in quantifying the effect of the pattern on wear. Even though a direct connection between the slide track pattern and wear has not yet been established, the slide track software makes it possible to investigate the effect of changing motion waveform amplitudes or phases, the Euler sequence, or of omitting certain waveforms to simplify the design of a simulator. By discretizing the load waveform, the integral $\int L\mathrm{d}x$ can be computed and used in calculating the wear factor k [12]. In the following, some examples of using the software are given.

Figure 11 shows how omitting either AA or IER waveforms changes the gait slide track pattern. If IER is left out, the narrow part of the force track and the other tracks in the middle of the pattern widens. Tracks near the equator and the vertical column of tracks in the middle become narrower. If AA is left out, the effect is nearly opposite. The force track and most of the tracks in the middle become narrow figures of eight, while the other tracks remain open loops. Consider designing a simulator starting from the gait waveforms [31] and with the Euler sequence for gait. In the light of Fig. 11, simplifying the three-axis walking motion to two-axis motion (to limit manufacturing costs of the design) is probably better done by omitting IER than AA. Omitting AA would result in a force track of high aspect ratio, which is likely to underestimate wear.

Figure 12 shows the effect of changing the Euler sequence on the shape of the force track of the HUT-3 simulator. In Fig. 12c, the thick line shows the track computed with the sequence IER$\rightarrow$AA$\rightarrow$FE, and the thin line shows the track computed with the sequence FE$\rightarrow$AA$\rightarrow$ IER. The tracks are clearly different in shape. The experimental verification showed that the former sequence was the right one for this simulator design.

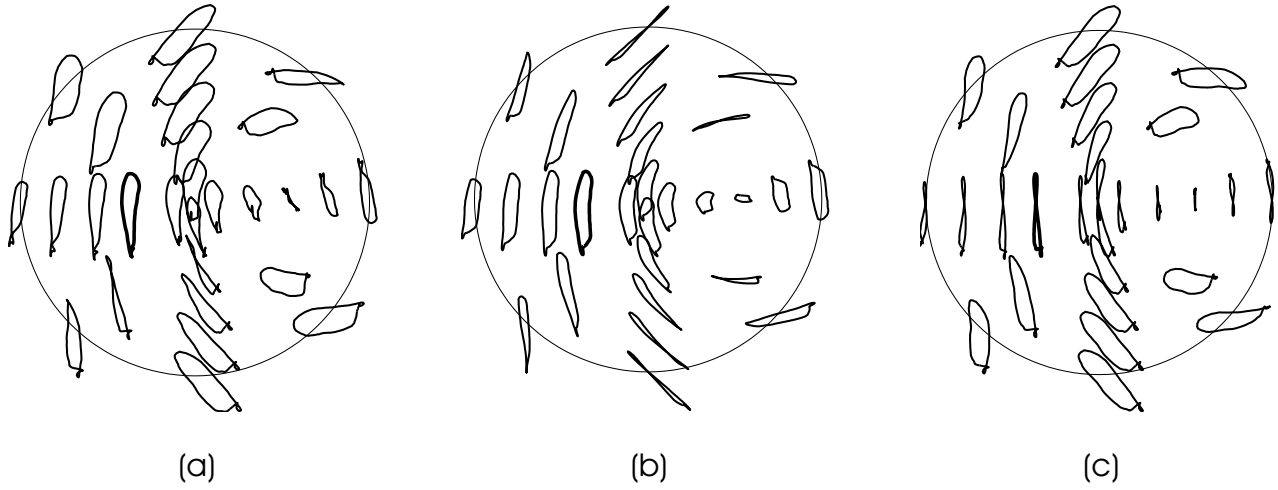

Figure 11. Effect of omitting IER or AA motion on the gait slide track pattern drawn on the femoral head. (a) All motion components included. Sequence was FE→AA→IER. (b) IER motion was omitted. Sequence was FE→AA. (c) AA motion was omitted. Sequence was FE→IER.

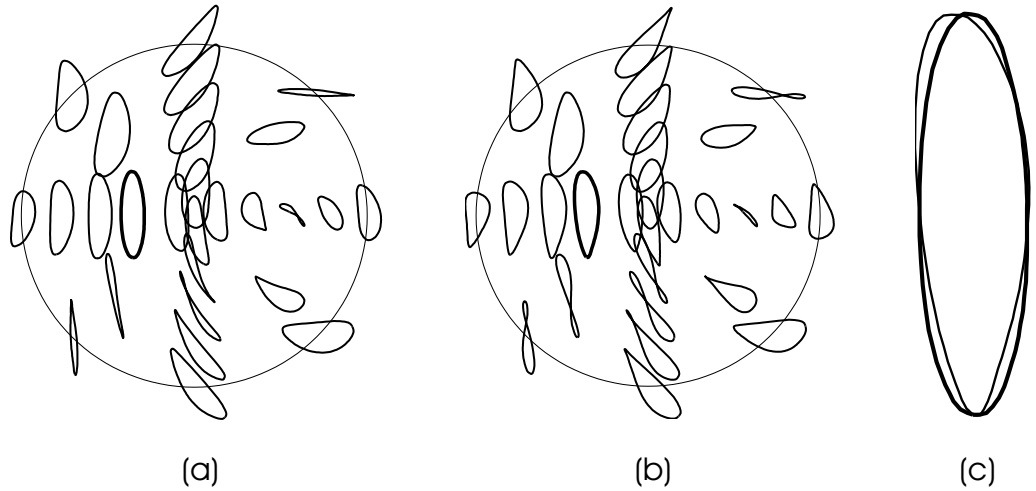

Figure 12. Effect of Euler sequence on shape of slide tracks of HUT-3 simulator. (a) Tracks computed with correct sequence for this simulator design, IER→AA→FE. Tracks have same shapes as tracks engraved in the simulator. Force track is shown with thick line. (b) Tracks computed with inverted sequence FE→AA→ IER. The shape of the tracks deviate from the shape of the correct tracks. Force track is shown with thick line. (c) The thick line shows the correct force track, while the thin line shows the force track computed with the inverted sequence.

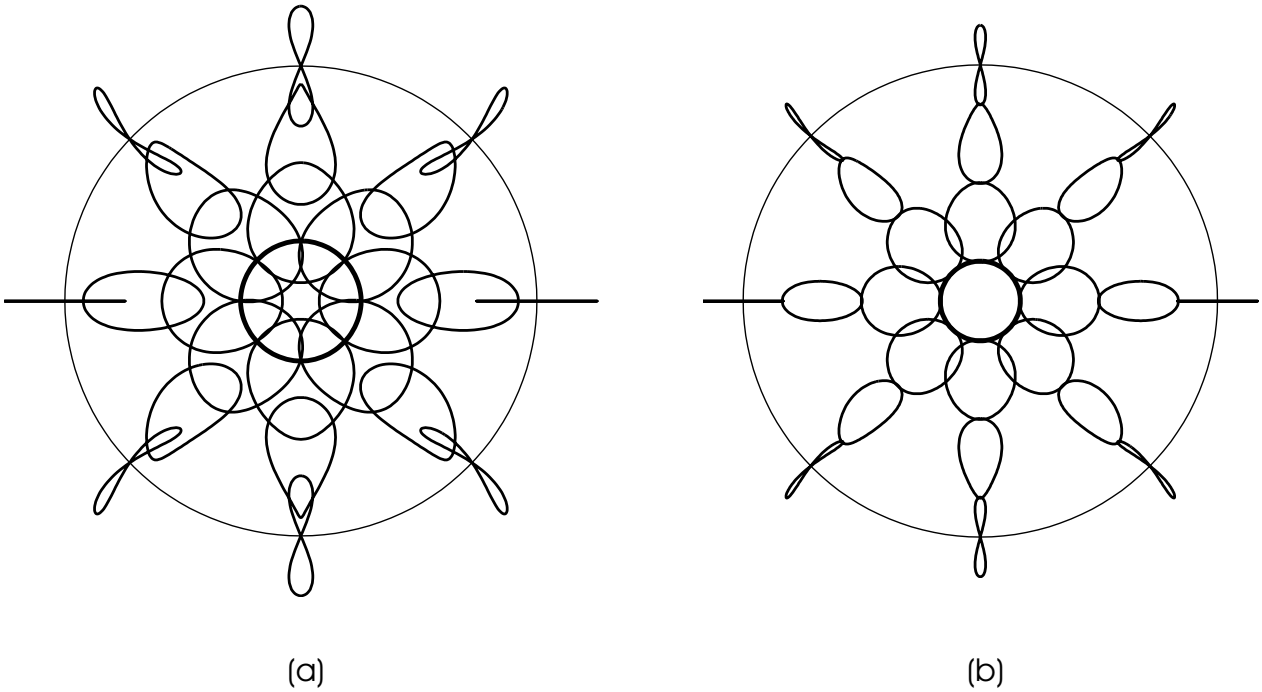

Figure 13. Slide tracks and force track (thick line) on femoral head in the HUT-BRM simulator. The effect of changing the inclination angle of the simulator is shown. (a) Tracks computed with standard inclination angle of 23°. The length of the force track was 2.46*r*. (b) Tracks computed with reduced inclination angle of 15.2°. The length of the force track was the same as in the simulation of gait, 1.65*r*.

Next, consider designing a zero-offset BRM simulator with a force track of the length computed for the gait waveforms (1.65*r*). Let the angle of inclination of the head be ψ. The length of the force track is $2\pi r\sin\psi = 2.46r$ because normally $\psi = 23°$ for the BRM simulator. Equating $2\pi r\sin\psi = 1.65r$, gives a new inclination angle $\psi = 15.2°$. Figure 13 shows the impact on the slide tracks of changing ψ from 23° to 15.2°.

In the ball-on-flat knee wear simulator, the articulation was non-conforming and the contact point moved cyclically relative to the polyethylene disk, such that the theoretical point of contact formed a narrow figure of eight. As a result of the rotation of the polyethylene disk, the direction of sliding was changing, which was manifested in detectable wear rates, even for non-irradiated and non-aged polyethylene (11–12 mg/10^6 cycles, Publication I). In trial tests with only the FE and APT motions, the relative motion was purely reciprocating, which resulted in too low wear rates (1 mg/10^6 cycles, Publication I).

5 CONCLUSIONS

This thesis treated the validation of wear simulation of prosthetic materials. The relative motion, and the polyethylene wear debris produced in different wear simulators were analyzed. The wear debris was isolated in thirteen different tests in four different wear simulators (Table IV and Publications I–IV). The slide tracks in walking and in a total of ten contemporary hip simulators (Publications V and VI), and in a knee wear simulator (Fig. 8) were computed. Based on this research, the following conclusions can be drawn:

1. The particle analyses showed that the simulators produced polyethylene wear particles in the same biologically active size range as particles isolated from tissues around hip and knee prostheses. Additionally, the morphologic features of the particles corresponded well, suggesting that the same basic wear mechanisms were acting in the simulators, as in the prosthetic hip and knee joints in vivo. Common to all wear tests was the fact that the lubricant was serum, or a lubricant based on albumin or γ-globulin, and that the relative motion was multidirectional. The slide track computations confirmed that the motion was multidirectional, because the instantaneous direction of sliding corresponded to the direction of the tangent of the slide track, and the open loop force tracks of the HUT-BRM and the HUT-3 simulators showed that the tangent to the track kept changing direction during the motion cycle. The multidirectionality of the sliding motion of the CTPOD simulator has been shown elsewhere [48]. In the ball-on-flat knee wear simulator, the slide track figure was a narrow figure of eight, showing that the motion was not purely reciprocating. All the simulators fulfilled the requirements concerning the state of the polyethylene bearing surface and the counterface, the wear factor, and the wear debris. In short, it can be concluded that the evaluated wear simulation methods were relevant for assessing wear of prosthetic joints.
2. The effect of the counterface surface roughness and the type of polyethylene (conventional or crosslinked) on the particle size distribution was strong. Against polished counterfaces, smaller particles were produced with crosslinked than with conventional polyethylene. The respective mean *ECD*-values were 0.10 μm and 0.21 μm. Against rough counterfaces, larger particles were produced. With both types of polyethylene, the mean *ECD*-value was approximately 0.4 μm. The effect on the particle size of increasing the counterface roughness was stronger with crosslinked polyethylene. A similar trend was found for the effect of counterface roughness on the wear factor (Publication III, Fig. 3), but against rough counterfaces the wear factor of crosslinked polyethylene was still an order of magnitude lower than that of conventional polyethylene.

3. The knee wear simulation (BOF) produced wear particles that were larger on the average than those produced in the hip wear simulations (CTPOD, BRM, HUT-3). The average *ECD*-value of the particles from the knee wear simulation was 0.69 μm, while the average *ECD*-value was less than or equal to 0.45 μm for the hip wear simulations.
4. The effect of the polished counterface surface material on the particle size distribution was weak. The mean *ECD*-values for particles produced with conventional polyethylene against alumina, CoCr and DLC coated CoCr, ranged from 0.27 μm to 0.33 μm. The corresponding wear factors ranged from 1.5 to 1.8 × 10^{-6} mm^3/Nm. Note however, that these results were obtained in the clean conditions of the laboratory. In the clinical situation, abrasive particles (e.g. bone cement) may be present, which would cause differences in the wear of polyethylene due to differences in the resistance of the counterfaces to abrasion. In addition, bone cement particles may be less prone to adhere to certain counterface materials (e.g. alumina [66]), which would further contribute to differences in polyethylene wear.
5. The lubricant protein content did not influence the particle size distribution. In the CTPOD tests with unirradiated polyethylene against stainless steel, the protein content of the lubricants ranged from 10 mg/ml to 73 mg/ml, while the mean *ECD*-value ranged from 0.37 μm to 0.38 μm. This was somewhat surprising, because the lubricant protein content is known to influence the *amount* of wear. A possible explanation is that the lubrication conditions and the wear mechanisms in these tests remained essentially the same, in the cited range of protein content.
6. The slide track software made it possible to visualize and analyze relative motion of the hip joint. In addition to computing slide tracks, it was possible to investigate the effect of changing the Euler sequence, or of omitting certain waveforms to simplify the design of a simulator. The effect of changes to the motion waveform amplitudes or phases, could be investigated by only generating new waveforms, i.e., without large modifications to the software. A basis for further research was established, because the software can be used to compute other quantities that are relevant for assessing wear, such as the sliding speed or the cyclic variation of the direction of sliding [12].
7. The slide track computations were valid, which was shown by experimental verifications done with the HUT-BRM and the HUT-3 simulators. The gait simulation (Publication V) and the tracks of other simulators (Publication VI) were computed according to the same principles as the verified tracks.

8. The slide track software provided a tool for comparing different hip simulator designs. By analyzing published data, it was possible to make a slide track overview of practically all contemporary hip simulators (Publication VI, together with Publication V). This was done by varying the Euler sequence, the motion waveforms and the force track marker point in the slide track software. The slide track overview showed that biaxial simulators omitting the abduction-adduction motion, had linear or high aspect ratio force tracks (Publication VI, Figs. 3f–h). When the abduction-adduction motion was omitted in the gait computations (Fig. 11), a similar effect was seen. In the three-axis simulators (and the purely biaxial HUT-BRM) the force tracks were open shapes (Publication VI, Figs. 3a–e; 4a–e,i). Thus, the simulators can be divided into two groups: those that omit and those that include the AA-motion. The differences between the two groups, in the shapes of the slide tracks in the high pressure regions of the articulation, may influence the wear results. High aspect ratio tracks indicated that the motion was nearly reciprocating, which is known to underestimate the polyethylene wear rate, compared to the clinical wear rate of polyethylene acetabular cups.
9. For the BRM (OBM) simulators, correct (experimentally verified) slide tracks were presented and it was shown that the shape of the rotation-prevention lever affected the slide track pattern (Publication V, Figs. 9 and 10). An offset rotation-prevention lever introduces IER motion, turning the simulator into a three-axis device (Publication VI).
10. For the HUT-3 simulator, it was shown that the overall pattern of slide tracks was similar to the pattern obtained in the slide track computation based on gait motion waveforms, and that the force track was elliptical (Publication V, Figs. 5 and 6). Computed simulator tracks were experimentally verified (Publication V, Figs. 6a and 7).
11. Simulators built according to the ISO/DIS 14242-1 standard (assuming a FE$\rightarrow$AA$\rightarrow$IER rotation sequence) would produce a slide track pattern with an elliptical force track and other open slide tracks on the center of contact (Publication VI, Fig. 3e), similar to the slide tracks present in the pattern of the HUT-3 simulator. The design requirement that the direction of sliding shall be continually changing would therefore be fulfilled by simulators meeting the ISO/DIS 14242-1 specifications. Note, however, that a similar slide track pattern was produced with only the FE and AA components of the gait motion (Fig. 11b), which suggests that the simulator need not be three-axial to obtain wear conditions similar to those specified in ISO/DIS 14242-1.

To make it possible to compare wear results produced with different simulators, future research efforts should be directed towards calculating an improved wear factor, for which the variations in the integral ∫Ldx, and the direction of sliding at different points on the articulating surface are taken into account. As a direct consequence of the present slide track research, the regular wear factor *k* can be computed for any hip simulator, by discretizing the load curve and evaluating the integral ∫Ldx for the force track [12]. This estimate can be improved by considering the pressure distribution, and summing the contributions of many slide tracks from all over the articulating surface. Another future improvement to incorporate in the calculation would be the effect of the variation in the direction of sliding along each track. However, wear tests under known conditions need to be done, to be able to quantify the effect of variations in relative motion on wear. Therefore, the same equipment, lubricant and loading should be used, with the force track shape as the only variable, to correlate the wear factor calculations with experimental results.

The most important research on wear simulation of artificial joints has so far been experimental and will most likely continue to be so in the future. However, computational wear simulation can become a valuable complement to wear tests, e.g., in predictions of the lifetime of prostheses, based on radiological measurements, patient activity, etc. To make computational wear simulation meaningful, better wear models are needed, and those can only be built on experimental facts, which calls for systematic experiments in which the relationships between the wear and the prosthetic material properties, relative motion, lubrication and loading are investigated.

REFERENCES

1. Ahlroos, T., Effect of lubricant on the wear of prosthetic joint materials. Doctoral dissertation, Acta Polytechnica Scandinavica, Me 153, Helsinki, The Finnish Academies of Technology, 2001.

2. Aspenberg, P. and Van der Vis, H., Migration, particles, and fluid pressure. A discussion of causes of prosthetic loosening. Clin Orthop Vol. 352 (1998), p. 75–80.

3. ASTM F04.16.09, Standard recommended practice for characterization of particles, Draft #3, 1 Dec 97. American Society for Testing and Materials, 1997.

4. Atkinson, J.R., Dowson, D., Isaac, J.H. and Wroblewski, B.M., Laboratory wear tests and clinical observations of the penetration of femoral heads into acetabular cups in total replacement hip joints. III: The measurement of internal volume changes in explanted Charnley sockets after 2–16 years in vivo and the determination of wear factors. Wear Vol. 104 (1985), p. 225–244.

5. Barbour, P.S.M., Stone, M.H., and Fisher, J., A hip joint simulator study using simplified loading and motion cycles generating physiological wear paths and rates. Proc Inst Mech Engr (H) J Eng Med Vol. 213 (1999), p. 455–467.

6. Barbour, P.S.M., Stone, M.H., and Fisher, J., A study of the wear resistance of three types of clinically applied UHMWPE for total replacement hip prostheses. Biomaterials Vol. 20 (1999), p. 2101–2106.

7. Bargmann, L.S., Bargmann, B.C., Collier, J.P., Currier, B.H. and Mayor, M.B., Current sterilization and packaging methods for polyethylene. Clin Orthop Vol. 369 (1999), p. 49–58.

8. Bauer, T.W. and Schils, J., The pathology of total joint arthroplasty II. Mechanisms of implant failure. Skeletal Radiol Vol. 28 (1999), p. 483–497.

9. Besong, A.A., Tipper, J.L. Mathews, B.J., Ingham, E., Stone, M.H. and Fisher, J., The influence of lubricant on the morphology of ultra-high molecular weight polyethylene wear debris generated in laboratory tests. Proc Inst Mech Engr (H) J Eng Med Vol. 213 (1999), p. 155–158.

10. Bragdon, C.R., O'Connor, D.O., Lowenstein, J.D., Jasty, M. and Syniuta, W.D., The importance of multidirectional motion on the wear of polyethylene. Proc Inst Mech Engr (H) J Eng Med Vol. 210 (1996), p. 157–165.

11. Bragdon, C.R., O'Connor, D.O., Lowenstein, J.D., Jasty, M. and Harris, W.H., Development of a new pin-on-disk testing machine for evaluating polyethylene wear. 24th Annual Meeting of the Society for Biomaterials, San Diego, 1998.

12. Calonius, O. and Saikko, V., Force track analysis of contemporary hip simulators. J Biomech, submitted for publication, January 2002.

13. Campbell, P., Ma, S., Yeom, B., McKellop, H., Schmalzried, T.P. and Amstutz, H.C., Isolation of predominantly submicron-sized UHMWPE wear particles from periprosthetic tissues. J Biomed Mater Res Vol. 29 (1995), p. 127–131.

14. Campbell, P., Doorn, P., Dorey, F. and Amstutz, H.C., Wear and morphology of ultra-high molecular weight polyethylene wear particles from total hip replacements. Proc Inst Mech Engr (H) J Eng Med Vol. 210 (1996), p. 167–174.

15. Cooper, J.R., Dowson, D. and Fisher, J., Macroscopic and microscopic wear mechanisms in ultra-high molecular weight polyethylene. Wear Vol. 162–164 (1993), p. 378–384.

16. Craig, J.J., Introduction to robotics: mechanics and control. Second edition. Reading, Addison-Wesley Publishing Company Inc., 1989.

17. Dowson, D., Wear oh where? Wear Vol. 103 (1985), p. 189–203.

18. Dowson, D., A comparative study of the performance of metallic and ceramic femoral head components in total replacement hip joints. Wear Vol. 190 (1995), p. 171–183.

19. Dowson, D., New joints for the Millennium: wear control in total replacement hip joints. Proc Inst Mech Engr (H) J Eng Med Vol. 215 (2001), p. 335–358.

20. Dowson, D. and Wallbridge, N.C., Laboratory wear tests and clinical observations of the penetration of femoral heads into acetabular cups in total replacement hip joints. I: Charnley prostheses with polytetrafluoroethylene acetabular cups. Wear Vol. 104 (1985), p. 203–215.

21. Dowson, D. and Jobbins, B., Design and development of a versatile hip joint simulator and a preliminary assessment of wear and creep in Charnley total replacement hip joints. Engineering in Medicine Vol. 17 (1988), p. 111–117.

22. Dumbleton, J.H., Tribology of natural and artificial joints. Amsterdam, Elsevier, 1981.

23. Eftekhar, N.S., The life and work of John Charnley. Clin Orthop Vol. 211 (1986), p. 10–22.

24. Elfick, A.P., Green, S.M., Pinder, M. and Unsworth, A., A novel technique for the detailed size characterization of wear debris. J Mater Sci: Mater Med Vol. 11 (2000), p. 267–271.

25. Goldsmith, A.A.J. and Dowson, D., A multi-station hip joint simulator study of the performance of 22 mm diameter zirconia–ultra-high molecular polyethylene total replacement hip joints. Proc Inst Mech Engr (H) J Eng Med Vol. 213 (1999), p. 77–90.

26. Goodman, S., Aspenberg, P., Song, Y., Knoblich, G., Huie, P., Regula, D., and Lidgren, L., Tissue ingrowth and differentiation in the bone-harvest chamber in the presence of cobalt-chromium-alloy and high-density-polyethylene particles. J Bone Joint Surg Vol. 77-A (1995), p. 1025–1035.

27. Green, T.R., Fisher, J., Stone, M., Wroblewski, B.M. and Ingham, E., Polyethylene particles of a ‘critical size’ are necessary for the induction of cytokines by macrophages in vitro. Biomaterials Vol. 19 (1998), p. 2297–2302.

28. Hall, R.M., Unsworth, A., Siney, P. and Wroblewski, The surface topography of retrieved femoral heads. J Mater Sci: Mater Med Vol. 7 (1996), p. 739–744.

29. Ingham, E. and Fisher, J., Biological reactions to wear debris in total joint replacement. Proc Inst Mech Engr (H) J Eng Med Vol. 214 (2000), p. 21–37.

30. ISO/DIS 14242-1 Draft International Standard, 2001. Implants for surgery – Wear of total hip joint prostheses – Part 1: Loading and displacement parameters for wear-testing machines and corresponding environmental conditions for test.

31. Johnston, R.C. and Smidt, G.L., Measurement of hip-joint motion during walking—evaluation of an electrogoniometric method. J Bone Joint Surg Vol. 51-A (1969), p. 1083–1094.

32. Klapperich, C., Komvopoulos, K. and Pruitt, L., Tribological properties and microstructure evolution of ultra-high molecular weight polyethylene. J Trib Vol. 121 (1999), p. 394–402.

33. Kobayashi, A., Bonfield, W., Kadoya, Y., et al: The size and shape of particulate polyethylene wear debris in total joint replacements. Proc Inst Mech Engr (H) J Eng Med Vol. 211 (1997), p. 11–15.

34. Kurtz, S.M., Muratoglu, O.K., Evans, M. and Edidin, A.A., Advances in the processing, sterilization, and crosslinking of ultra-high molecular weight polyethylene for total joint arthroplasty. Biomaterials Vol. 20 (1999), p.1659–1688.

35. Lancaster, J.K., Basic mechanisms of friction and wear of polymers. Plastics & Polymers Vol. 41 (1973), p.297–306.

36. McEvoy, A., Jeyam, M., Ferrier, G., Evans, C.E. and Andrew, J.G., Synergistic effect of particles and cyclic pressure on cytokine production in human monocyte/macrophages: proposed role in periprosthetic osteolysis. Bone Vol. 30 (2002), p. 171–177.

37. McKellop, H.A., Campbell, P., Park, S-H., Schmalzried, T.P., Grigoris, P., Amstutz, H.C. and Sarmiento, A., The origin of submicron polyethylene wear debris in total hip arthroplasty. Clin Orthop Vol. 311 (1995), p. 3–20.

38. McKellop, H., Shen, F., DiMaio, W. and Lancaster, J.G., Wear of gamma-crosslinked polyethylene acetabular cups against roughened femoral balls. Clin Orthop Vol. 369 (1999), p. 73–82.

39. Muratoglu, O.K., Bragdon, C.R., O'Connor, D.O., Jasty, M., Harris, W.H., Gul, R. and McGarry, F., Unified wear model for highly crosslinked ultra-high molecular weight polyethylenes (UHMWPE). Biomaterials Vol. 20 (1999), p. 1463–1470.

40. Nevalainen, J., Hirvonen, A. and Pulkkinen, P., The 1998–1999 implant yearbook on orthopaedic endoprostheses. Vantaa, National Agency for Medicines, 2000.

41. Peterson, C., Benjamin, J.B., Szivek, J.A., Anderson, P.L., Shriki, J. and Wong, M., Polyethylene particle morphology in synovial fluid of failed knee arthroplasty. Clin Orthop Vol. 359 (1999), p. 167–175.

42. Pienkowski, D., Jacob, R., Hoglin, D., Saum, K., Kaufer, H. and Nicholls, P.J., Low-voltage scanning electron microscopic imaging of ultrahigh-molecular-weight polyethylene. J Biomed Mater Res Vol. 29 (1995), p. 1167–1174.

43. Ramamurti, B.S., Bragdon, C.R., O'Connor, D.O., Lowenstein, J.D., Jasty, M., Estok, D.M. and Harris, W.H., Loci of movement of selected points on the femoral head during normal gait. The Journal of Arthroplasty Vol. 11 (1996), p. 845–852.

44. Ramamurti, B.S., Estok, D.M., Jasty, M. and Harris, W.H., Analysis of the kinematics of different hip simulators used to study wear of candidate materials for the articulation of total hip arthroplasties. Journal of Orthopaedic Research Vol. 16 (1998), p. 365–369.

45. Revell, P.A., Al-Saffar, N. and Kobayashi, A., Biological reaction to debris in relation to joint prosthesis. Proc Inst Mech Engr (H) J Eng Med Vol. 211 (1997), p.187–197.

46. Russ, J.C., The image processing handbook. Boca Raton, CRC Press Inc., 1992.

47. Saikko, V., A three-axis hip joint simulator for wear and friction studies on total hip prosthesis. Proc Inst Mech Engr (H) J Eng Med Vol. 210 (1996), p. 175–185.

48. Saikko, V., A multidirectional motion pin-on-disk wear test method for prosthetic joint materials. J Biomed Mater Res Vol. 41 (1998), p. 58–64.

49. Saikko, V. and Ahlroos, T., Type of motion and lubricant in wear simulation of polyethylene acetabular cup. Proc Inst Mech Engr (H) J Eng Med Vol. 213 (1999), p. 301–310.

50. Saikko, V. and Ahlroos, T., Wear simulation of UHMWPE for total hip replacement with multidirectional motion pin-on-disk device: Effects of counterface material, contact area, and lubricant. J Biomed Mater Res Vol. 49 (2000), p. 147–154.

51. Saikko, V., Effect of lubricant protein concentration on the wear of ultrahigh molecular weight polyethylene. Submitted for publication (2002).

52. Saikko, V. and Calonius, O., Wear of conventional and crosslinked ultrahigh molecular weight polyethylene acetabular cups against polished and roughened CoCr femoral heads in a biaxial hip simulator. J Biomed Mater Res Appl Biomater (2002), in press.

53. Schmalzried, T.P., Campbell, P., Schmitt, A.K., Brown, I.C. and Amstutz, H.C., Shapes and dimensional characteristics of polyethylene wear particles generated in vivo by total knee replacements compared to total hip replacements. J Biomed Mater Res Appl Biomater Vol. 38 (1997), p. 203–210.

54. Scott, M., Widding, K. and Jani, S., Do current wear particle isolation procedures underestimate the number of particles generated by prosthetic bearing components? Wear Vol. 251 (2001), p. 1213–1217.

55. Shanbhag, A.S., Jacobs, J.J., Glant, T.T., Gilbert, J.L., Black, J. and Galante, J.O., Composition and morphology of wear debris in failed uncemented total hip replacement. J Bone Joint Surg Vol. 76B (1994), p. 60–67.

56. Shanbhag, A.S., Bailey, H.O., Hwang, D.S., et al., Quantitative analysis of ultrahigh molecular weight polyethylene (UHMWPE) wear debris associated with total knee replacements. J Biomed Mater Res Appl Biomater Vol. 53 (2000), p. 100–110.

57. Smith, S.L. and Unsworth, A., A five-station hip joint simulator. Proc Inst Mech Engr (H) J Eng Med Vol. 215 (2001), p. 61–64.

58. Sochart, D.H., Relationship of acetabular wear to osteolysis and loosening in total hip arthroplasty. Clin Orthop Vol. 363 (1999), p. 135–150.

59. Ungethüm, M., Tribologisch-biomechanische Untersuchungen für den totalen Gelenkersatz der menschlichen Hüfte. Doctoral Dissertation. Rheinisch-Westfälische Technische Hochschule Aachen, 1976.

60. Wang, A., Stark, C. and Dumbleton, J.H., Mechanistic and morphological origins of ultra-high molecular weight polyethylene wear debris in total joint replacement prostheses. Proc Inst Mech Engr (H) J Eng Med Vol. 210 (1996), p. 141–155.

61. Wang, A., Essner, A., Stark, C. and Dumbleton, J.H., Comparison of the size and morphology of UHMWPE wear debris produced by a hip joint simulator under serum and water lubricated conditions. Biomaterials Vol. 17 (1996), p. 865–871.

62. Wang, A., Polineni, V.K., Essner, A., Sokol, M., Sun, D.C., Stark, C. and Dumbleton, J.H., The significance of nonlinear motion in the wear screening of orthopaedic implant materials. J Testing Eval Vol. 25 (1997), p. 239–245.

63. Wang, A., Sun, D.C., Yau, S.-S., Edwards, B., Sokol, M., Essner, A., Polineni, V.K., Stark, C. and Dumbleton, J.H., Orientation softening in the deformation and wear of ultra-high molecular weight polyethylene. Wear Vol. 203–204 (1997), p. 230–241.

64. Wang, A., Essner, A., Polineni, V.K., Stark, C. and Dumbleton, J.H., Lubrication and wear of ultra-high molecular weight polyethylene in total joint replacements. Trib Int Vol. 31 (1998), p. 17–33.

65. Wang, A., Polineni, V.K., Essner, A., Stark, C. and Dumbleton, J.H., Role of proteins and hylauronic acid in the lubrication and wear of UHMWPE acetabular cups. 24th Annual Meeting of the Society for Biomaterials, San Diego, California, April 22–26, 1998.

66. Wang, A. and Essner, A., Three-body wear of UHMWPE acetabular cups by PMMA particles against CoCr, alumina and zirconia heads in a hip simulator. Wear Vol. 250 (2001), p. 212–216.

APPENDIX A. COMPUTATION OF SLIDE TRACKS

A brief summary of the slide track computations is given. See Fig. 3 for an overview. A more detailed presentation of the computations was given in Publication V, Appendix A.

Definitions

XYZ	Reference coordinate system, fixed relative to acetabular cup
xyz	Moving coordinate system, fixed relative to femoral head
$\xi\eta$	Coordinate system fixed to center of flattened hemisphere of articulating surface
j	Unit vector index; j = 1,2,3
$\mathbf{u}^j$	Unit vectors in the directions of the axes of *xyz* coordinate system ($\mathbf{u}^1$, $\mathbf{u}^2$, $\mathbf{u}^3$)
$\mathbf{U}^j$	Unit vectors in the directions of the axes of *XYZ* coordinate system ($\mathbf{U}^1$, $\mathbf{U}^2$, $\mathbf{U}^3$)
S	Sequence of rotations made about moving axes, e.g., FE$\rightarrow$AA$\rightarrow$IER
N	Number of discrete points in rotation angle vectors
i	Index to discretized motion waveforms; i = 1,2,3,…,*N*
α_i, β_i, γ_i	Rotation angles of point i of discretized FE, AA and IER waveforms
r	Radius of spherical articulating surface
$\mathbf{r}_0$	Position vector of marker point in neutral (initial) position
$\mathbf{r}_i$	Position vector of marker point after rotations according to α_i, β_i, γ_i and sequence **S**
$\mathbf{R}(\alpha_i,\beta_i,\gamma_i;\mathbf{S})$	Rotation matrix corresponding to angles α_i, β_i, γ_i and sequence **S**. See, e.g., [16]
c_{xY}	Direction cosine for axes *x* and *Y*, $c_{xY} = \cos(\mathbf{u}^1,\mathbf{U}^2)$; similarly for other axes
$\mathbf{L}=\mathbf{L}(\mathbf{u}^j,\mathbf{U}^j)$	Matrix containing the direction cosines of angles between the axes of *xyz* and *XYZ*

$$\mathbf{L} = \begin{bmatrix} c_{xX} & c_{xY} & c_{xZ} \\ c_{yX} & c_{yY} & c_{yZ} \\ c_{zX} & c_{zY} & c_{zZ} \end{bmatrix}$$

Cup tracks

The marker point fixed to the head was repeatedly rotated from its neutral (initial) position $\mathbf{r}_0$ to a new position on the slide track. Each point at position $\mathbf{r}_i$ on the slide track corresponded to one set of rotation angles (α_i,β_i,γ_i). In order to avoid the accumulation of numerical errors, the points were not computed by using the previous point on the track as a starting point.

Each slide track point was computed with the following rotation:

$$\mathbf{r}_i = \mathbf{R}(\alpha_i,\beta_i,\gamma_i;\mathbf{S})\ \mathbf{r}_0 \qquad \text{(A1)}$$

The track was drawn on the cup surface by connecting all points defined by $\mathbf{r}_i$.

Head tracks

The marker points were fixed to the cup. The displacement of a marker point relative to the moving head, was computed from the relative orientation of the coordinate systems *XYZ* and *xyz*, using the direction cosine matrix **L**. In the neutral position, the orientation of the axes coincided, i.e., $\mathbf{u}_0^1 = \mathbf{U}^1$, $\mathbf{u}_0^2 = \mathbf{U}^2$ and $\mathbf{u}_0^3 = \mathbf{U}^3$. The new orientation of the head coordinate system *xyz*, and the corresponding $\mathbf{L}_i$ was computed with

$$\mathbf{u}_i^j = \mathbf{R}(\alpha_i, \beta_i, \gamma_i; \mathbf{S})\mathbf{u}_0^j \qquad \text{(A2)}$$

$$\mathbf{L}_i = \mathbf{L}(\mathbf{u}_i^j, \mathbf{u}_0^j) \qquad \text{(A3)}$$

For each marker point, the track positions were computed by repeatedly applying the set of angles $(\alpha_i,\beta_i,\gamma_i)$:

$$\mathbf{r}_i = \mathbf{L}_i\ \mathbf{r}_0 \qquad \text{(A4)}$$

The track was drawn on the head surface by connecting all points defined by Eq. A4. Note that cup tracks can be produced with the same method as the head tracks, but by transposing $\mathbf{L}_i$ ($\mathbf{r}_i = \mathbf{L}_i^T\ \mathbf{r}_0$).

Flattening

The slide tracks were flattened by transforming the three-dimensional cartesian coordinates of the slide track points into spherical coordinates, which were subsequently transformed into polar coordinates (Figure 14). The neutral positions of the marker points were used as base points for transforming the separate tracks ('local' flattening). In polar coordinates, the radial distance of a track point from the base point was equal to the distance between the two points, measured along the spherical surface. The positions of the base points were transformed into polar coordinates with respect to the pole of the articulating surface. The flattened tracks were drawn around the positions determined by the polar coordinates of the base points. The flattened hemisphere of the articulation was drawn as a circle with a diameter of πr.

The flattening operations were done after transforming the articulating surface, with all base points and tracks, to the normal orientation, where the pole was located on the *Z*-axis of the reference coordinate system (Fig. 14a). In Publication V, Figs. 5a, 6a and 8a, the femoral head was shown in this orientation. For local flattening of a separate track, the base point was rotated onto the *Z*-axis. The same rotations were applied to the track points associated with the base point, such that the track points became located around the pole (Fig. 14b). The *XYZ* coordinates of the track points were then transformed to spherical coordinates: $(X,Y,Z)_i \rightarrow (r,\Phi,\Theta)_i$, where r = radius of head or cup, Φ = angle in *X*,*Y*-plane and Θ = angle from the *Z*-axis. The polar coordinates were calculated as $(s,\phi)_i = (r\Theta,\Phi)_i$. The flattened coordinates of the base point were calculated in the same manner from the coordinates $(X,Y,Z)_{BP}$ that the base point had, before it was rotated onto the *Z*-axis (Fig. 14a): $(s_{BP},\Phi_{BP}) = (r\Theta_{BP},\Phi_{BP})$. A plane coordinate system, ξη, was fixed to the center point of the flattened hemisphere of the articulation. The polar coordinates were transformed to plane coordinates: $(s_{BP},\Phi_{BP}) \rightarrow (\xi,\eta)_{BP}$ and $(s,\phi)_i \rightarrow (\xi,\eta)_i$. The track points $(\xi,\eta)_i$ were moved from around the origin to around the base point $(\xi,\eta)_{BP}$ (Fig. 14c), after which the track was drawn by connecting the points $(\xi,\eta)_i$. The process was repeated for each track to produce the flattened track pattern.

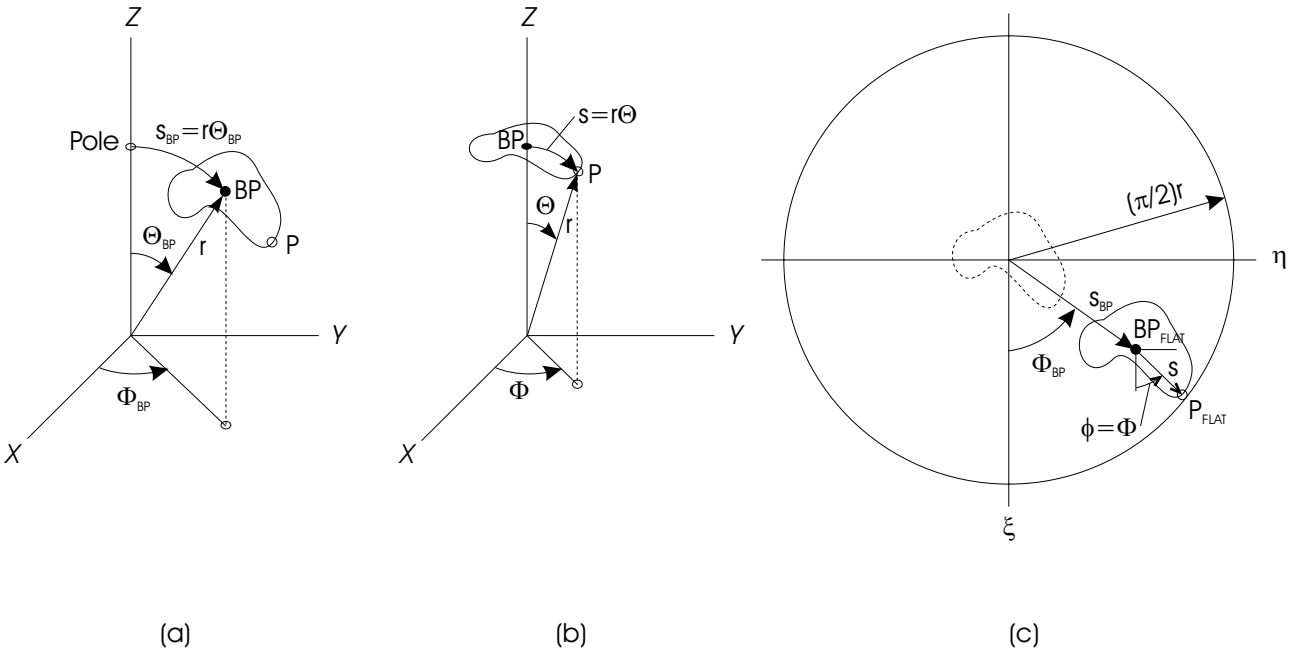

Figure 14. Flattening of slide track on spherical surface of radius *r*. XY-plane coincides with equatorial plane and Z-axis passes through the pole. (a) Slide track with base point (BP) and arbitrary track point (P) shown. For BP, spherical coordinates and distance from pole along surface, are indicated. (b) BP rotated to pole and same rotations applied to track points. For P, spherical coordinates and distance from pole along surface, are indicated. (c) Location of flattened track shown within circle representing flattened hemisphere.